Inorganic Chemistry
Cite This: Inorg. Chem. 2019, 58, 3895−3909
Article
pubs.acs.org/IC

Combinatorial Synthesis to Identify a Potent, Necrosis-Inducing Rhenium Anticancer Agent

Chilaluck C. Konkankit,[†] Brett A. Vaughn,[§] Samantha N. MacMillan,[†] Eszter Boros,[§] and Justin J. Wilson*[,†]

[†]Department of Chemistry and Chemical Biology, Cornell University, Ithaca, New York 14853, United States
[§]Department of Chemistry, Stony Brook University, Stony Brook, New York 11794, United States

Supporting Information

ABSTRACT: Combinatorial synthesis can be applied for developing a library of compounds that can be rapidly screened for biological activity. Here, we report the application of microwave-assisted combinatorial chemistry for the synthesis of 80 rhenium(I) tricarbonyl complexes bearing diimine ligands. This library was evaluated for anticancer activity in three different cancer cell lines, enabling the identification of three lead compounds with cancer cell growth-inhibitory activities of less than 10 μM. These three lead structures, **Re-9B**, **Re-9C**, and **Re-9D**, were synthesized independently and fully characterized by NMR spectroscopy, mass spectrometry, elemental analysis, and X-ray crystallography. The most potent of these three complexes, **Re-9D**, was further explored to understand its mechanism of action. Complex **Re-9D** is equally effective in both wild-type and cisplatin-resistant A2780 ovarian cancer cells, indicating that it circumvents cisplatin resistance. This compound was also shown to possess promising activity against ovarian cancer tumor spheroids. Additionally, flow cytometry showed that **Re-9D** does not induce cell cycle arrest or flipping of phosphatidylserine to the outer cell membrane. Analysis of the morphological changes of cancer cells treated with **Re-9D** revealed that this compound gives rise to rapid plasma membrane rupture. Collectively, these data suggest that **Re-9D** induces necrosis in cancer cells. To assess the in vivo biodistribution and stability of this compound, a radioactive ^{99m}Tc analogue of **Re-9D**, **^{99m}Tc-9D(H_2O)**, was synthesized and administered to naïve BALB/c mice. Results of these studies indicate that **^{99m}Tc-9D(H_2O)** exhibits high metabolic stability and a distinct biodistribution profile. This research demonstrates that combinatorial synthesis is an effective approach for the development of new rhenium anticancer agents with advantageous biological properties.

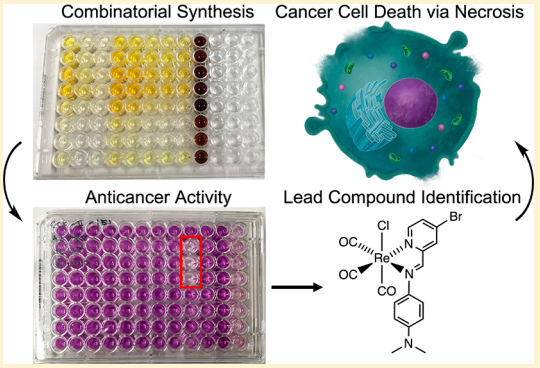

INTRODUCTION

Ovarian cancer is a leading cause of death for women worldwide.[1] The dismal five-year survival rate for ovarian cancer has only improved marginally since 1977. The current standard of care for this disease is the combination chemotherapy regimen of either cisplatin or carboplatin and taxanes, such as paclitaxel and docetaxel.[2] Despite the widespread success and implementation of these platinum-based drugs, their use for ovarian cancer is limited by the fact that ∼70% of patients relapse with the disease returning in a form that is platinum-resistant.[3,4] Resistance to cisplatin is multifactorial; resistant cancer cells exhibit a combination of increased capacity for DNA repair, decreased drug uptake, and increased ability to sequester and deactivate drugs with biomolecules such as glutathione (GSH).[5−11] As such, the design of alternative metal-based anticancer agents that are not susceptible to these platinum resistance mechanisms is a promising approach for the development of new drugs for the treatment of ovarian cancer.

The investigation of alternative anticancer metal complexes has led to the discovery of compounds of titanium, gold, and ruthenium that exhibit promising anticancer activity,[12] with several of these agents advancing to clinical trials.[13−16] Transition metal-based drug candidates containing the 5d elements, rhenium, osmium, and iridium, can also exhibit effective anticancer properties.[17,18] Among these candidates, rhenium-based anticancer agents containing the stable rhenium(I) tricarbonyl motif were recently found to be particularly promising.[19−21] These complexes are kinetically inert and exhibit rich spectroscopic properties, features that make them appealing for biological use. For example, we have demonstrated that particular candidates from this class of compounds exhibit potent in vitro anticancer activity and can be used for luminescence imaging in cells.[22,23] Furthermore, technetium-99m (^{99m}Tc), the most commonly employed diagnostic radionuclide in nuclear medicine, exhibits similar chemistry to rhenium, allowing the synthesis of ^{99m}Tc homologues of promising rhenium anticancer drug candidates that can be used for in vivo imaging and biodistribution studies.[24]

Received: December 20, 2018
Published: February 22, 2019

DOI: 10.1021/acs.inorgchem.8b03552
Inorg. Chem. 2019, 58, 3895−3909

Collectively, these properties demonstrate the promise of rhenium complexes as theragnostic anticancer agents.

Although recent reports have highlighted the promising anticancer activity of several rhenium complexes,[18−20] access to larger libraries of these compounds is limited by conventional synthetic approaches and the high cost of rhenium starting materials. The application of combinatorial synthetic strategies[25,26] would substantially reduce time and effort in developing a library of these complexes for biological use. Combinatorial syntheses typically require one-pot reactions that combine different building blocks to access a set of diverse molecular entities.[26−29] In the context of medicinal inorganic chemistry, combinatorial approaches have been applied to generate libraries of anticancer ruthenium and platinum complexes.[30−37] Importantly, these studies identified promising anticancer drug candidates, validating the use of combinatorial chemistry for the discovery of new inorganic therapeutic agents.

Given the successful application of combinatorial synthesis for the discovery of new platinum and ruthenium anticancer agents, we sought to apply this methodology to identify rhenium-based anticancer drug candidates. For this study, we employed a one-pot, three-component reaction involving an aniline, an aldehyde with an attached N-donor, and $Re(CO)_5Cl$ to rapidly synthesize an array of rhenium(I) tricarbonyl complexes bearing different diimine ligands. These complexes were then screened for anticancer activity in a panel of cancer cell lines. Through these studies, we identified a new lead compound, **Re-9D**, and evaluated its biological mechanism of action. Collectively, this study further validates the implementation of combinatorial chemistry approaches for the discovery of new metal-based drug candidates with different mechanisms of action.

RESULTS AND DISCUSSION

Microwave-Assisted One-Pot Combinatorial Synthesis. With the objective of developing a library of rhenium compounds through combinatorial synthesis, we sought chemistry that is robust enough to be performed in a 96-well plate, yet offers a diverse range of structural possibilities. A previously reported approach for the combinatorial synthesis of anticancer ruthenium-arene complexes exploited the metal-templated condensation of anilines with picolinaldehydes to yield new compounds bearing pyridylimine ligands.[30,31] Based on the promising anticancer activities of rhenium(I) tricarbonyl complexes, we aimed to adapt this condensation chemistry for the generation of a diverse library of these compounds. The feasibility of this strategy was bolstered by previous studies that have demonstrated that $Re(CO)_5Cl$ acts as an appropriate template for aniline-picolinaldehyde condensation chemistry to afford rhenium(I) tricarbonyl complexes bearing pyridylimine ligands.[38−41]

To apply this chemistry in a combinatorial manner, we envisioned mixing three components, namely, an aldehyde, an aniline, and $Re(CO)_5Cl$, in each well of a 96-well plate (Figure 1a). By varying both the aldehyde and the aniline, a diverse range of compounds containing functional groups of differing lipophilicities and electron-donating properties can be accessed. Such structural variety could aid efforts to determine a structure−activity relationship (SAR) for this class of compounds.[42−45] We employed series of anilines (**1**−**10**) and aldehydes (**A**−**H**) and administered them to different columns and rows, respectively, of a 96-well plate (Figure 1b). Within the 96-well plate, these components were incubated with $Re(CO)_5Cl$ in dimethyl sulfoxide (DMSO). The reactions did not

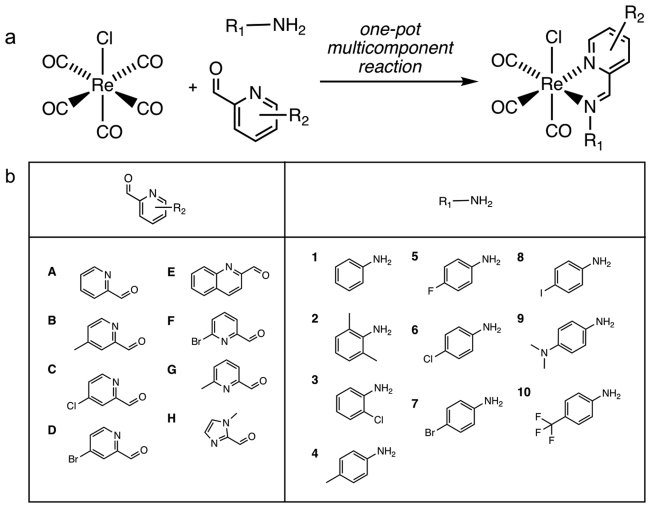

Figure 1. (a) General synthetic approach for rhenium-diimine formation. (b) Aldehydes (**A**−**H**) and anilines (**1**−**10**) with different functional groups used as starting materials for imine condensation in library synthesis.

proceed neither at room temperature nor at 37 °C. However, upon the application of microwave radiation for 5 min, the desired reactivity was observed, as indicated by dramatic color changes in the solutions within the wells (Figure S1a, Supporting Information). Notably, the use of microwave irradiation for the synthesis of related rhenium(I) tricarbonyl complexes with pyridylpyrazole ligands has recently been described.[46] The efficacy of these 96-well three-component reactions was assessed by high-performance liquid chromatography (HPLC) coupled to an autosampler (representative chromatogram Figure S1b, Supporting Information). Of the 80 reactions performed, 12% of them had formed the desired products in a purity of greater than 70%, reflecting the general success of this synthetic strategy. For comparison, 15% of the initial combinatorially synthesized library of ruthenium-arene pyridylimine complexes were obtained in greater than 70% purity.[30]

Biological Activity Screening of Compound Library. With the combinatorial library of rhenium-diimine complexes in hand, they were next evaluated for anticancer activity in a panel of cancer cell lines comprising cervical (HeLa), ovarian (A2780), and cisplatin-resistant ovarian (A2780CP70) cancers. The compounds in this library were directly transferred to 96-well plates containing the cancer cells, achieving a final administered concentration of 10 μM (1% DMSO). The cytotoxicities of the 80 compounds at this single 10 μM dose were evaluated to rapidly identify potential lead compounds using 3-(4,5-dimethylthiazol-2-yl)-2,5-diphenyltetrazolium bromide (MTT).[47] From these single-dose studies, three compounds, **Re-9B**, **Re-9C**, and **Re-9D**, were found to induce greater than 95% cell death relative to control cells treated with 1% DMSO only at 10 μM (Table S1, Figures 2 and S2, Supporting Information). The extent of cell death caused by other compounds in the library ranged from less than 5% to 81%, indicating that the nature of the diimine ligands plays an important role in modulating the biological activities of this class of compounds. To determine the SAR for these compounds, we analyzed both the calculated water−octanol partition coefficients (log P), a quantitative measure of lipophilicity (Table S2, Supporting Information),[42,43] and the Hammett substituent

DOI: 10.1021/acs.inorgchem.8b03552
Inorg. Chem. 2019, 58, 3895−3909

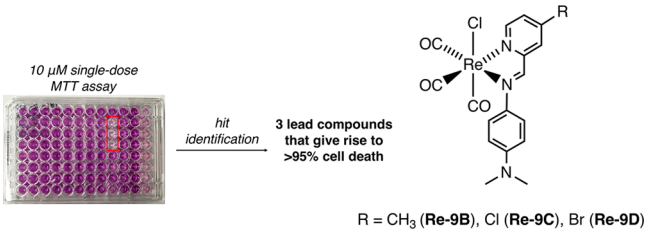

Figure 2. MTT cell viability assay of the 80 combinatorially synthesized rhenium-diimine complexes at a single-dose of 10 μM (1% DMSO). This initial screen identified **Re-9B**, **Re-9C**, and **Re-9D** as lead candidates. In the MTT assay, viable cells generate a purple formazan dye, whereas nonviable cells do not.

parameters, quantitative measures of electron-donating and -withdrawing properties (Table S3, Supporting Information),[44,45,48] for the different diimine ligands. Unfortunately, analyses of these parameters do not indicate any clear SAR that are predictive of compound cytotoxicity. The most active compounds, **Re-9B**, **Re-9C**, and **Re-9D**, however, all share in common the strongly electron-donating dimethylamino substituent on the aniline, suggesting that this structural feature is important for their cytotoxic properties. Another common structural feature of these three lead compounds is the presence of a substituent in the para position of the picolinaldehyde. Rhenium compounds that contain the dimethylamino functionality but lack a para substituent on the aniline are inactive. Thus, both features appear to be requisite for effective anticancer activity within this class of compounds.

Synthesis and Characterization of Lead Compounds. Having established **Re-9B**, **Re-9C**, and **Re-9D** as the most active compounds in our combinatorial screening, we sought to synthesize them on a preparative scale, validate their purities, and explore their biological properties in greater detail. The large-scale syntheses of these compounds were performed as one-pot reactions following previously reported methods.[38] The ligand components, aniline **9** and aldehyde **B**, **C**, or **D**, were allowed to stir in MeOH for 20 min to form the desired free ligands **9B**, **9C**, or **9D**. The addition of $Re(CO)_5Cl$ to these solutions at reflux afforded red solutions from which **Re-9B**, **Re-9C**, or **Re-9D** could be isolated upon evaporation of the MeOH and subsequent recrystallization using diethyl ether.

These compounds were characterized by ^{1}H NMR spectroscopy, Fourier transform infrared (FTIR) spectroscopy, UV−vis spectroscopy, electrospray ionization mass spectrometry (ESI-MS), elemental analysis (EA), and reversed-phase HPLC (RP-HPLC). The free ligands (**9B**, **9C**, and **9D**) were also separately synthesized and characterized by ^{1}H NMR spectroscopy, ESI-MS, and EA. The ^{1}H NMR spectra of the complexes display resonances of the aromatic and imine peaks that are shifted further downfield compared to the free ligands. (Figures S3−S8, Supporting Information). The IR spectra (Figures S9−S12, Supporting Information) reveal three intense C≡O stretching modes. The two low-energy modes range in energy from 1905 to 1928 cm^{-1}, and the third stretching mode is observed at ∼2025 cm^{-1}. The observation of three peaks is expected for the rhenium(I) tricarbonyl core in a C_1-symmetric ligand environment, and their energies are consistent with previously reported complexes of this type.[38] The UV−vis spectra of the complexes in acetonitrile (ACN) display two prominent features. A higher-energy peak between 260 and 270 nm is assigned to an intraligand $\pi-\pi^*$ transition, and a lower-energy band between 460 and 490 nm is assigned to a metal-to-ligand charge transfer (MLCT) transition. Notably, the MLCT transition of **Re-9B** (λ_{max} = 461 nm) is lower in energy compared to those of **Re-9C** and **Re-9D** (both with λ_{max} = 486 nm). The red-shift observed in **Re-9B** correlates with the presence of the electron-donating methyl group on the aniline in **9B**, in contrast to the electron-withdrawing halide groups in **9C** and **9D**. Lastly, the complexes were characterized by ESI-MS, confirming their molecular formula through the observation of a predominant m/z peak corresponding to the $[M-Cl + DMSO]^+$ ion. The complex purity was verified to be greater than 95% by both EA and RP-HPLC analysis (Figures S14−S16, Supporting Information).

With these compounds fully characterized, their stability in aqueous buffer and in the presence of serum was investigated. For these studies, **Re-9D** was used as a representative example of the three compounds. When **Re-9D** is incubated in aqueous buffer (0.1% DMSO, 100 mM MOPS, pH 7.4), its spectral feature at 530 nm undergoes a blue-shift over the course of several hours (Figure S17a, Supporting Information). The final spectral trace is consistent with that of the aquated form of **Re-9D**, **Re-9D(H$_2$O)**, which was prepared in situ via the reaction of **Re-9D** with AgOTf. Thus, this result shows that **Re-9D** undergoes aquation on the time scale of hours in a manner that is similar to cisplatin, for example. We performed this same experiment in the presence of serum (0.1% DMSO, 10% fetal bovine serum (FBS), 100 mM MOPS, pH 7.4) as well (Figure S17b, Supporting Information). Likewise, the final UV−vis spectrum was consistent with that of **Re-9D(H$_2$O)**, indicating

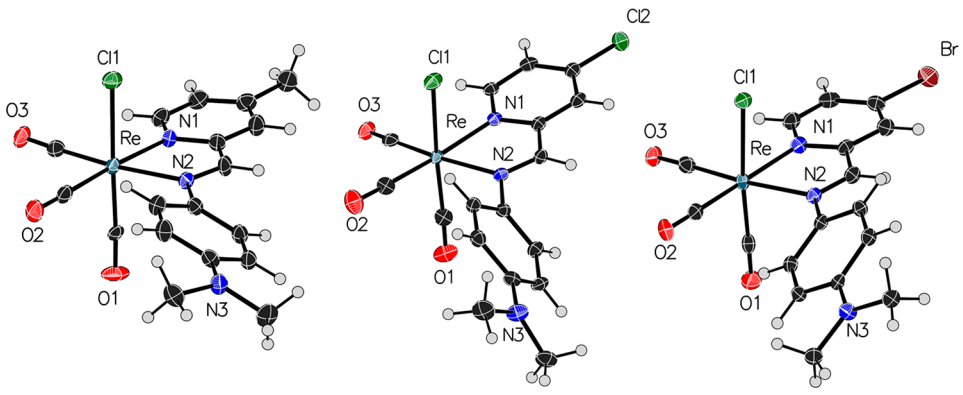

Figure 3. X-ray crystal structures of **Re-9B**, **Re-9C**, and **Re-9D**. The disordered components of the axial Cl and CO ligands are omitted for clarity. Thermal ellipsoids are drawn at the 50% probability level.

DOI: 10.1021/acs.inorgchem.8b03552
Inorg. Chem. 2019, 58, 3895−3909

that, even in the presence of serum, aquation occurs with no detectable further compound decomposition. Furthermore, the time-scale of aquation in the presence and absence of serum was nearly identical. Thus, although **Re-9D** is susceptible to aquation, it is otherwise stable in aqueous solution.

Single-Crystal X-ray Diffraction. Complexes **Re-9B**, **Re-9C**, and **Re-9D** were also characterized structurally by single-crystal X-ray diffraction. The crystal structures of these complexes are shown in Figure 3, and relevant crystallographic parameters are detailed in Table S4 (Supporting Information). Selected interatomic distances and angles are presented in Table 1. All complexes exhibit the expected octahedral geometry around the d^6 rhenium(I) center with the carbonyl ligands arranged in a facial manner. The Re−N_1 and Re−N_2 interatomic distances range from 2.171 to 2.179 Å and from 2.185 to 2.215 Å, respectively. These values are similar to those observed in the previously reported crystal structure of *fac*-[Re(CO)$_3$(**1A**)Cl],[41] suggesting that the peripheral substituents on the pyridylimine ligands have a negligible influence on Re−N interatomic distances. The Re−C and C−O distances are consistent with the expected results for this class of compounds. Positional disorder between the axial chloride and CO ligands was detected and modeled in **Re-9B** and **Re-9D**. Therefore, the accuracy of axial distances (Re−CO_{axial} and Re−Cl) is less reliable than the other metrics in these structures. Notably, the pyridylimine ligands in all three structures are not planar. The aniline ring is tilted from the plane of the chelate ring with torsion angles that range from −59.49 to 35.25°. This deviation from planarity may be a consequence of steric repulsion between the ortho hydrogen atom on the aniline and the adjacent CO ligand. Lastly, the dimethylamino substituent is planar in all three structures, indicating that the nitrogen center is sp^2 hybridized and in conjugation with the aromatic ring system.

Table 1. Selected Interatomic Distances (Å) and Angles (deg) for Re-9B, Re-9C, and Re-9D[a]

	Re-9B	Re-9C	Re-9D
Re−N_1	2.171(2)	2.179(3)	2.176(5)
Re−N_2	2.215(3)	2.185(3)	2.209(5)
Re−Cl_1	2.422(5)[b]	2.4837(9)	2.4776(2)[b]
Re−C_1	1.9421(13)[b]	1.907(4)	1.926(7)[b]
Re−C_2	1.931(3)	1.919(4)	1.926(6)
Re−C_3	1.916(3)	1.925(5)	1.915(7)
Cl_1−Re−C_1	177.8(5)[b]	173.55(12)	175.0(2)[b]
Re−N_2−C_{10}−C_{15}	−28.99	−59.49	35.25

[a]Atoms are labeled as shown in Figure 3. Numbers in parentheses are the estimated standard deviations for the last significant figure. [b]These bond distances and angles are affected by disorder.

In Vitro Anticancer Activity of Lead Compounds. Having independently synthesized and fully characterized the three lead compounds identified from our combinatorial screening, we sought to evaluate their in vitro anticancer activities via dose-escalation studies in wild-type (A2780) and cisplatin-resistant ovarian cancer (A2780CP70) cells. Furthermore, the anticancer properties of the ligand components and free ligands were evaluated to verify that the observed activities of our identified lead compounds were due to the complexes rather than residual starting materials. (Figures S18−S40, Supporting Information). All three rhenium complexes exhibit 50% growth inhibitory concentration (IC_{50}) values below 10 μM after a 48 h treatment period (Figure 4a), whereas the starting components (**9**, **B**, **C**, and **D**) and free ligands (**9B**, **9C**, and **9D**) induce 50% cell death at concentrations exceeding 10 μM. The rhenium starting material, $Re(CO)_5Cl$, is also known to not induce any cytotoxic effects in cancer cells at concentrations under 200 μM,[49] indicating that this compound is not likely a contributing factor to the activities observed. The IC_{50} values for all samples in A2780 and A2780CP70 cell lines are shown in Table 2. The enhanced cytotoxic activities of the rhenium compounds compared to the free ligands or ligand components suggest that the combinatorial screening accurately identified the intact complexes as potential lead candidates. All three complexes are not cross-resistant with cisplatin, as evidenced by the fact that they kill wild-type and cisplatin-resistant cell lines with equal efficacy (Figure 4b).

Among the three compounds, **Re-9D** is the most potent as characterized by an IC_{50} value of ~3 μM in these ovarian cancer cell lines. On the basis of the promising activity of **Re-9D**, we evaluated this compound further in HeLa cervical cancer cells and noncancerous HEK293 human embryonic kidney fibroblasts (Table 3, Figures S18 and S41−44, Supporting Information). In comparison to cisplatin, **Re-9D** is more active against the HeLa cells, confirming this compound's cytotoxic potential. However, **Re-9D** also exhibits a low micromolar IC_{50} value in the noncancerous HEK293 kidney cells. Although this compound is equally toxic in HEK293 and HeLa cells, note that

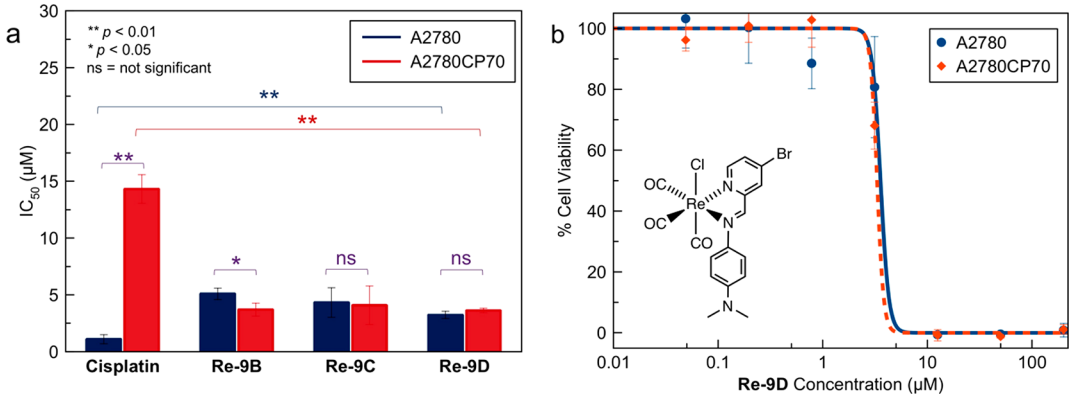

Figure 4. (a) IC_{50} values of cisplatin and lead rhenium compounds in A2780 (blue) and A2780CP70 (red) cells. The error bars represent the standard deviation from three independent experiments. (b) Dose−response curves for **Re-9D** in A2780 (blue) and A2780CP70 (red) cell lines. The error bars represent the standard deviation from six replicates.

DOI: 10.1021/acs.inorgchem.8b03552
Inorg. Chem. 2019, 58, 3895−3909

Table 2. IC_{50} Values (μM) for Cisplatin, Starting Components, Free Ligands, and Lead Compounds in A2780 and A2780CP70 Cells[a]

	A2780	A2780CP70
cisplatin	1.1 ± 0.4	14.3 ± 1.3
9	37.2 ± 13.1	37.4 ± 10.8
B	61.5 ± 19.3	152.5 ± 98.7
C	71.5 ± 20.4	76.8 ± 26.1
D	33.7 ± 10.8	58.0 ± 36.1
9B	37.5 ± 13.1	15.8 ± 1.8
9C	39.4 ± 15.8	47.1 ± 1.7
9D	25.4 ± 7.2	22.4 ± 5.7
Re-9B	5.1 ± 0.5	3.7 ± 0.6
Re-9C	4.3 ± 1.3	4.1 ± 1.7
Re-9D	3.2 ± 0.3	3.6 ± 0.2

[a]The errors represent the standard deviation from three independent experiments.

Table 3. IC_{50} Values (μM) for Cisplatin and Re-9D[a]

	HeLa	HEK293
cisplatin	9.8 ± 0.9	2.7 ± 1.8
Re-9D	3.4 ± 1.0	3.4 ± 0.1

[a]The errors represent the standard deviation from three independent experiments.

cisplatin is actually 3.6 times more effective in killing the noncancerous kidney cells. Therefore, the in vitro therapeutic window of this compound is larger than that of cisplatin. Given its poor selectivity for cancer cells, continued compound optimization, possibly via the addition of tumor-targeting moieties, will be required to further minimize the toxicity of **Re-9D** in noncancerous cells.

Notably, the shapes of the dose–response curves for cells treated with **Re-9D** consistently display a large gradient at the inflection point. The steepness of the dose–response curve, known as the Hill slope (HS), has potential implications on the mechanism of action of the compound.[50,51] For example, compounds that give rise to large HS values are less sensitive to cell-to-cell variation that arises within a sample due to differences in the cell cycle progression and protein expression levels.[52−55] For comparison, the dose–response curves of cisplatin-treated cells are shallow and have Hill slope values that are close to 1. By contrast, **Re-9D** gives rise to substantially larger HS values between 10 and 15 across A2780, A2780CP70, HeLa, and HEK293 cell lines. These large HS values imparted by **Re-9D** may indicate that this compound induces cell death in a manner that is independent of the cell-to-cell variability. Further comparative analysis, however, is required to better understand how the dose–response curve shape affects anticancer activity and what the implications are with respect to the mode of cell death.[55]

The in vitro studies described above demonstrate that **Re-9D** is effective at killing cancer cells when cultured as two-dimensional (2D) monolayers. However, this 2D model does not accurately capture the properties of solid three-dimensional (3D) tumors found in vivo.[56] To evaluate the anticancer activity of **Re-9D** in a more biologically relevant model, 3D tumor spheroids, which share a number of features with solid tumors found in vivo,[57,58] were employed. Tumor spheroids (250–300 μm in diameter) comprising A2780 cells[57] were treated with either cisplatin or **Re-9D**, and their viability was determined using the resazurin cell viability assay (Figure 5).[59−61] The resulting dose–response curves reveal IC_{50} values of 2.4 and 6.9 μM for cisplatin and **Re-9D**, respectively (Figure 5). In contrast to the monolayer model, complete cell death was not observed in the tumor spheroids even at the highest concentrations of cisplatin and **Re-9D** administered, demonstrating how the compounds are less active in this 3D model. This result is consistent with previous studies that similarly shows cisplatin to fail at inducing 100% cell death in 3D tumor spheroids.[62] This lack of complete cell death may arise from the inabilities of these compounds to penetrate and access the central interior of the tumor spheroid. Continuous treatment with the compounds may potentially lead to complete spheroid dissolution, but this approach is likely to be most effective for smaller tumor spheroid models.

Effects of GSH on Cell Viability. As demonstrated above, **Re-9D** is able to circumvent cisplatin resistance in the A2780 ovarian cancer cells. Because cisplatin resistance is multifactorial, we sought to understand the origin of the lack of cross-resistance of **Re-9D** with cisplatin. One major phenotype of cisplatin-resistant cells is the presence of elevated levels of intracellular GSH.[9,63] This biomolecule exhibits antioxidant activity and can also bind and sequester foreign metal ions and complexes, such as cisplatin.[64] The deactivation of metal-based drug candidates by GSH is a common cause of multifactorial resistance by cells. As such, there is significant interest in the development of new agents that are not susceptible to deactivation by GSH, a

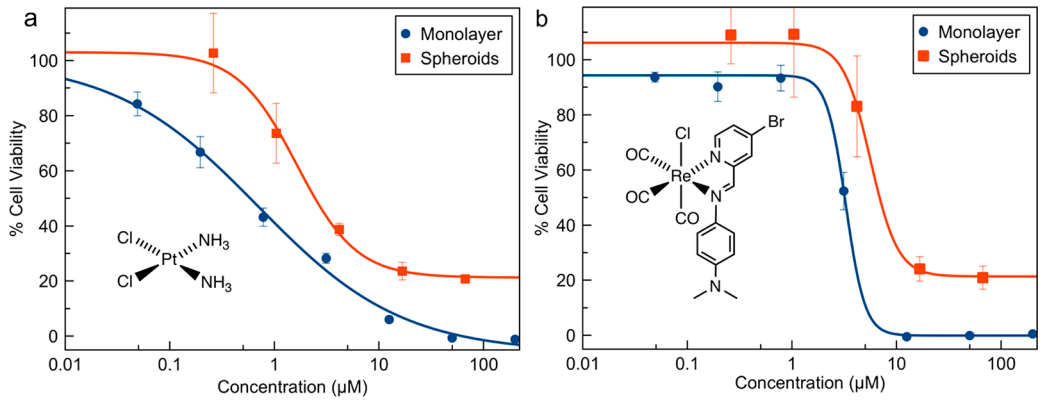

Figure 5. Dose–response curves of A2780 cell monolayers (blue) and tumor spheroids (red) treated with (a) cisplatin or (b) **Re-9D**. The error bars represent the standard deviation from six replicates.

DOI: 10.1021/acs.inorgchem.8b03552
Inorg. Chem. 2019, 58, 3895−3909

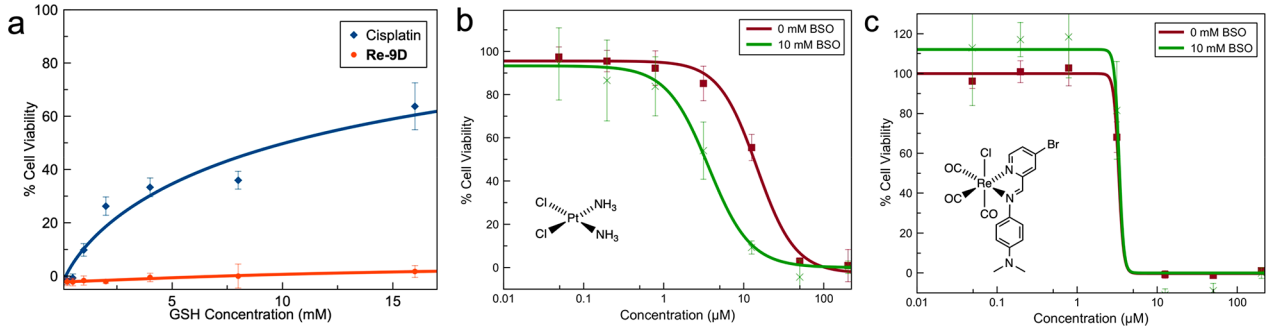

Figure 6. (a) Dose−response curves of A2780CP70 cells in the presence of either 100 μM **Re-9D** (red) or cisplatin (blue) and increasing concentrations of GSH. The data show how GSH protects cells from cisplatin but not **Re-9D**. (b) Dose−response curves for cisplatin-treated A2780CP70 cells in the absence (burgundy) or presence of 10 mM BSO (green). (c) Dose−response curves for **Re-9D**-treated A2780CP70 cells in the absence (burgundy) or presence of 10 mM BSO (green). The error bars represent the standard deviation from six replicates.

property that has been observed in several metal-based compounds.[65−67] To evaluate the role of GSH in inhibiting the cytotoxic activity of **Re-9D**, A2780CP70 cells were treated with 100 μM of this compound and given varying concentrations of GSH, ranging from 0.25 to 16 mM. Increasing GSH had a negligible effect on the viability of cells treated with **Re-9D** (Figure 6a). By contrast, the cytotoxic activity of cisplatin was significantly diminished in the presence of higher concentrations of GSH. These data support the hypothesis that **Re-9D** is not deactivated by GSH extracellularly.

To further verify this result and confirm that **Re-9D** is not deactivated by intracellular GSH, we performed viability studies in the presence of L-buthionine sulfoximine (BSO), which is a selective inhibitor of γ-glutathione synthetase, the enzyme responsible for intracellular GSH production. On the basis of its ability to decrease intracellular GSH levels, BSO has been shown to enhance the cytotoxic effects of metal-based drugs.[64,65,67−72] A2780CP70 cells were treated with 10 mM BSO to deplete intracellular glutathione concentrations and then incubated with varying concentrations of cisplatin or **Re-9D**. Upon preincubation of the cells with BSO, cisplatin exhibits greater potency, as evidenced by a lower IC_{50} value of 4.7 μM (Figure 6b). By contrast, the activity of **Re-9D** is not affected by the depletion of GSH by BSO (Figure 6c). This result provides further evidence against the role of GSH in altering the anticancer activity of **Re-9D**. Collectively, these results suggest that GSH is unable to effectively sequester the rhenium(I) center of this compound. They further imply that **Re-9D** does not induce cell death via the production of reactive oxygen species (ROS), because the antioxidant activity of GSH can effectively protect cells against this type of cytotoxic insult as well.

Cellular Uptake and Localization Analysis of Re-9D and Cisplatin. Another key feature of cisplatin resistance is decreased drug uptake.[73] Effective cell uptake is required for metal-based drug candidates to induce cancer cell death. The ability of transition metal compounds to penetrate the cell membrane can be quantified using graphite furnace atomic absorption spectroscopy (GFAAS) or inductively coupled plasma mass spectrometry (ICP-MS),[74−77] and these data can provide insight on the efficacy of a compound for killing cells. Additionally, many compounds of rhenium have been analyzed for their localization in cells using confocal fluorescence microscopy, providing information on their biotargets and mechanisms of action.[20,78,79] Because **Re-9D** is not luminescent, the cellular uptake and localization of this compound and cisplatin for comparative purposes in both A2780 and A2780CP70 cells was analyzed with GFAAS and ICP-MS. Following a modified version of previously described methods, cells were incubated with 10 μM **Re-9D** or 10 μM cisplatin for 24 h, and the different lysate samples were isolated and analyzed for their metal content normalized by the amount of protein in the samples.[80] These results are compiled in Table 4. For cells

Table 4. Cellular Fractionation Uptake Data Quantified Using GFAAS (Platinum) and ICP-MS (Rhenium)[a]

	cell fraction	metal content[b] in A2780 cells (ng/μg protein)	metal content[b] in A2780CP70 cells (ng/μg protein)
cisplatin	whole cell[c]	0.086 ± 0.004	0.045 ± 0.001
	nuclei[d]	0.059 ± 0.003	0.023 ± 0.001
	mitochondria[e]	0.069 ± 0.005	0.032 ± 0.002
Re-9D	whole cell[c]	0.17 ± 0.01	0.10 ± 0.01
	nuclei[d]	0.25 ± 0.01	0.26 ± 0.12
	mitochondria[e]	1.01 ± 0.26	1.13 ± 0.28

[a]Protein content was determined with BCA assays. [b]The errors represent the standard error from three independent experiments. [c]Metal content is normalized to the amount of protein from whole cells. [d]Metal content is normalized to the amount of protein from nuclei. [e]Metal content is normalized to the amount of protein from mitochondria.

treated with cisplatin, lower quantities of platinum were detected in the resistant A2780CP70 cells in comparison to the wild-type A2780 cells. These data are consistent with previous studies that also demonstrate that there is lower platinum uptake in cisplatin-resistant ovarian cancer cells compared to the wild-type A2780 cells.[81] Notably, samples treated with **Re-9D** exhibit statistically similar rhenium accumulation in nuclear and mitochondrial lysates between both A2780 and A2780CP70 cell lines. However, the whole cell uptake of rhenium is ∼40% lower in the A2780CP70 cells compared to the A2780 cells. These results suggest that of the cellular uptake of **Re-9D** is negatively affected by the alterations to the ovarian cancer cells that contribute to their resistance. The observation that the nuclear and mitochondrial fraction in both cells lines contain similar content of rhenium, however, suggests that decreased overall cell uptake does not prevent this compound from reaching these organelles in equal concentrations. In comparing the mitochondrial and nuclear fraction, it is apparent that **Re-9D** preferentially accumulates in the mitochondria.

DOI: 10.1021/acs.inorgchem.8b03552
Inorg. Chem. 2019, 58, 3895−3909

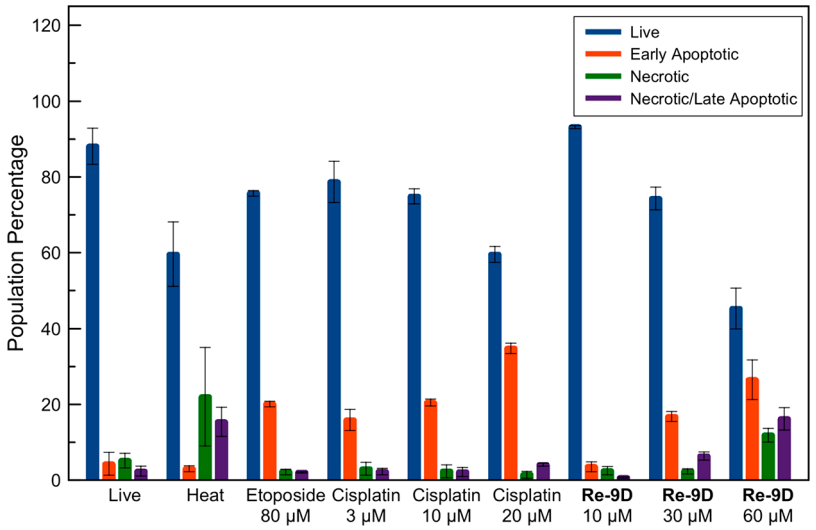

Figure 7. Averaged populations of A2780 cells treated with heat (10 min at 60 °C), etoposide, cisplatin, or **Re-9D**. The error bars represent the standard deviation from three independent experiments.

Flow Cytometry. Having determined that **Re-9D** can overcome cisplatin resistance, its mechanism of action was further investigated to understand how it induces cancer cell death. A number of anticancer agents disrupt regulation of the cell cycle in a manner that reflects their mechanism of action.[82] For example, cisplatin arrests the cell cycle in the S and G2/M phases by inhibiting DNA transcription.[83,84] Using propidium iodide (PI) and flow cytometry, we evaluated the ability of **Re-9D** to alter the cell cycle. PI is luminescent only when bound to DNA, and the intensity of intracellular luminescence, as measured by flow cytometry, is proportional to the amount of DNA within the cell.[85] Cells in the G0/G1 phase have one full copy of DNA, whereas cells in the G2/M phase have two copies of the chromosomal DNA. Cells in the S phase have an intermediate number of copies of DNA. Hence, the use of PI to quantify the amount of DNA can indicate the phase of the cell cycle that each cell is in. Treatment of A2780 cells with 5 μM cisplatin for 24 h showed stalling in the S and G2/M phases, consistent with previous studies (Figure S45a,b, Supporting Information).[86] By contrast, treatment with 5 μM **Re-9D** for 24 h minimally stalls the G0/G1 phase (78.5%) compared to the untreated cells (73.8%). The lack of a substantial effect on the cell cycle suggests that **Re-9D** acts in a manner that is independent of the cell cycle status. This result argues against direct DNA targeting as a mechanism of action for this compound, because DNA-targeting drugs are known to be heavily dependent on the phase of the cell cycle.[87] Additionally, regulated forms of cell death, such as apoptosis, often rely on specific checkpoints within the cell cycle to mediate these processes. By contrast, unregulated cell death, namely, necrosis, is expected to be largely independent of the cell cycle. For a related previously reported rhenium(I) tricarbonyl complex, cancer cells were found to be stalled in the G2/M phase.[22] A comparison of the results for these compounds reveals that the biological properties of rhenium(I) tricarbonyl complexes exhibit a remarkable dependence on the natures of their supporting ligands.

The mechanism of action of **Re-9D** was further evaluated for its ability to induce apoptosis by determining the extent to which this compound causes externalization of phosphatidylserine (PS) to the outer cell membrane. PS is a plasma membrane phospholipid that is predominately located on the inner membrane of the cell.[88] A hallmark feature of apoptotic cell death is the rotation of this phospholipid to the outer leaflet of the cell membrane. Therefore, apoptotic cells can be identified using annexin V, a protein with a high binding affinity and selectivity for exposed PS,[89] conjugated to a fluorescent dye (annexin V−Alexa Fluor 488). Additionally, PI can be used to stain necrotic cells, which are characterized by their permeabilized outer membranes.[89] The simultaneous use of PI and dye-labeled annexin V enables the differentiation of cells undergoing apoptosis or necrosis in response to a cytotoxic agent. A2780 cells were treated with **Re-9D** and analyzed via flow cytometry in conjunction with these two dyes to determine apoptotic and necrotic cell populations (Figure 7). As control experiments, cells were treated with etoposide or cisplatin, subjected to high temperatures (60 °C, 10 min), and analyzed in a similar manner.[90] As expected, on the basis of their abilities to induce apoptosis, both etoposide- and cisplatin-treated samples all show increased annexin V-positive cell populations as compared to the untreated control. Likewise, cells subjected to increased temperatures were characterized by a PI-positive population, confirming the expected necrotic cell death under these conditions. By contrast, cells treated with 10 μM **Re-9D** did not display a significant increase in annexin V binding. At higher concentrations of 30 μM and 60 μM **Re-9D**, annexin V- and PI-positive cell populations increased. The distinct separation of these populations, as shown in the density plots (Figure S46, Supporting Information), is poor. The lack of clear distinction between these populations suggests that the annexin V-positive populations may be arising downstream of cell permeabilization induced by necrotic cell death.

Live Cell Imaging and Time-Lapse Microscopy. To further probe the mechanism of cell death induced by **Re-9D**, morphological changes in A2780CP70 cells treated with this compound were investigated using optical microscopy. Characteristic morphological features of apoptotic cell death include cell shrinkage, membrane blebbing, and nuclear fragmentation.[91] By contrast, necrosis leads to the loss of cell membrane integrity, resulting in expulsion of intracellular contents.[92−94] Upon treatment of A2780CP70 cells with 60 μM **Re-9D** (Figure 8, Video S1, Supporting Information),

DOI: 10.1021/acs.inorgchem.8b03552
Inorg. Chem. 2019, 58, 3895−3909

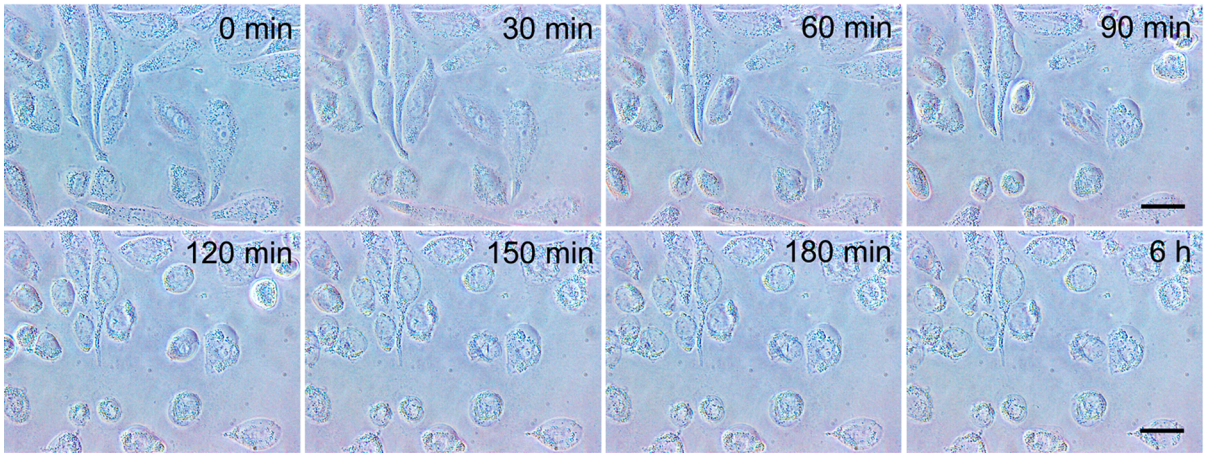

Figure 8. Brightfield time-lapse microscopy images of A2780CP70 cells using an optical microscope showing changes in cellular morphology after treatment with 60 μM **Re-9D**. Scale bars = 100 μm.

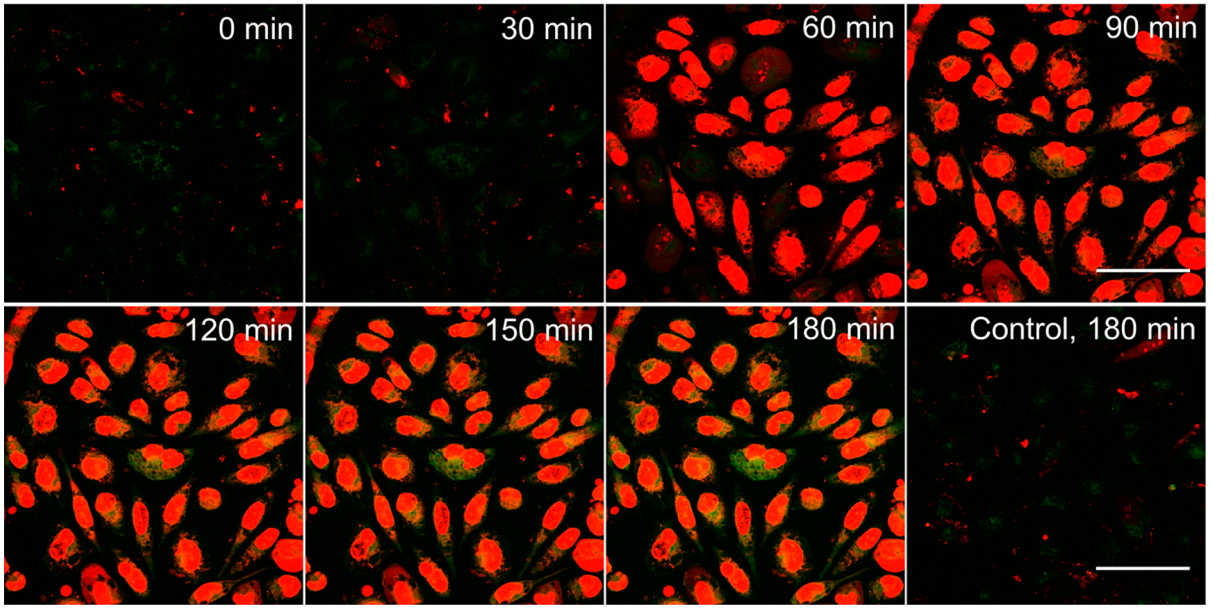

Figure 9. Time-lapse microscopy images of A2780CP70 cells using a confocal fluorescent microscope showing cellular autofluorescence (green) and PI (red) after treatment with 60 μM **Re-9D**. Scale bars = 100 μm.

microscopy revealed changes in cell morphology within 90 min of incubation. Specifically, the majority of cells were rounded, and cytoplasmic expulsion was observed. The changes were distinct from untreated control cells, for which only minor morphological differences were observed (Figure S47, Supporting Information). The similarities in the morphological changes induced by **Re-9D** and other agents known to give rise to necrosis supports the conclusion that this rhenium complex exhibits cell death via necrosis.

As an additional validation of necrotic cell death, we employed PI as a marker for necrosis in conjunction with fluorescence microscopy. As membrane integrity is lost during necrosis, PI can enter the cells and bind to nuclear DNA, eliciting a fluorescence emission increase. A2780CP70 cells treated with 60 μM **Re-9D** in the presence of PI were monitored by confocal fluorescence microscopy over 3 h (Figure 9, Video S2, Supporting Information). Within 60 min of incubation, the majority of cells exhibited intense red luminescence of PI, indicating that the cell membrane integrity was lost over this time period. These results further confirm that **Re-9D** induces necrosis. The rapidity at which **Re-9D** induces necrosis (less than 2 h) is noteworthy. An organic drug candidate, AG311, which exhibits its anticancer activity through mitochondrial dysfunction, was similarly shown to induce necrosis within a short time period.[93,95]

In Vivo Biodistribution and Metabolite Analysis. An advantage of using rhenium compounds as anticancer agents is the widespread availability of ^{99m}Tc, an imaging radionuclide that possesses similar chemical properties as rhenium. Complexes of ^{99m}Tc that are structurally analogous to promising rhenium drug candidates can be synthesized and used as in vivo companion diagnostic agents for single-photon emission computed tomography (SPECT) imaging.[96−98] To evaluate the potential of a companion imaging agent for **Re-9D**, we synthesized the analogous radionuclide-based complex of the formula $[^{99m}\mathrm{Tc}(\mathbf{9D})(\mathrm{CO})_3(\mathrm{H_2O})]^+$ (^{99m}**Tc-9D**($\mathbf{H_2O}$)). As described below, our synthetic procedures led to isolation of this aqua-capped species instead of a chlorido-capped compound, which would be more strictly analogous to **Re-9D**. The difference in complex charge may lead to distinct

DOI: 10.1021/acs.inorgchem.8b03552
Inorg. Chem. 2019, 58, 3895−3909

biodistribution patterns for these two compounds. Because **Re-9D** undergoes aquation, however, we expect that at longer time points these compounds may exhibit similar biodistribution patterns. Further data are needed to confirm this hypothesis, but the in vivo data of ^{99m}**Tc-9D(H$_2$O)** is an initial step in this direction.

Compound ^{99m}**Tc-9D(H$_2$O)** was prepared from Na-[^{99m}TcO$_4$] and Na$_2$[H$_3$BCO$_2$] to form [^{99m}Tc(CO)$_3$(OH$_2$)$_3$]$^+$ (Scheme S1, Supporting Information).[99] This trisaqua precursor was subsequently treated with ligand **9D** for 40 min at 50 °C to obtain the desired ^{99m}**Tc-9D(H$_2$O)** complex, confirmed to contain the axial aqua ligand by HPLC (Figure S48, Supporting Information), in a 48% radiochemical yield. Subsequently, the compound was purified using preparative RP-HPLC to 99% radiochemical purity and was formulated for in vivo injection. Cohorts (n = 3, 4) of naïve BALB/c mice were injected with ^{99m}**Tc-9D(H$_2$O)**, and the percent injected dose per gram (% ID/g) biodistribution was determined at 30, 60, and 120 min time points (Figure 10 and Table S5, Supporting Information). The results of these biodistribution studies reveal that this compound clears through both renal and hepatic pathways, consistent with observations for related technetium-(I) tricarbonyl complexes including [^{99m}Tc(CO)$_3$(2,9-dimethyl-1,10-phenanthroline)(H$_2$O)]$^+$ that was previously studied in our lab.[22,100,101] Additionally, ^{99m}**Tc-9D(H$_2$O)** exhibits elevated uptake in the myocardium compared to [^{99m}Tc(CO)$_3$(2,9-dimethyl-1,10-phenanthroline)(H$_2$O)]$^+$. Given the large concentration of mitochondria in cardiac cells, this increased uptake in the heart is consistent with cellular fractionation studies, described above, which show high concentrations of **Re-9D** observed in the mitochondria.

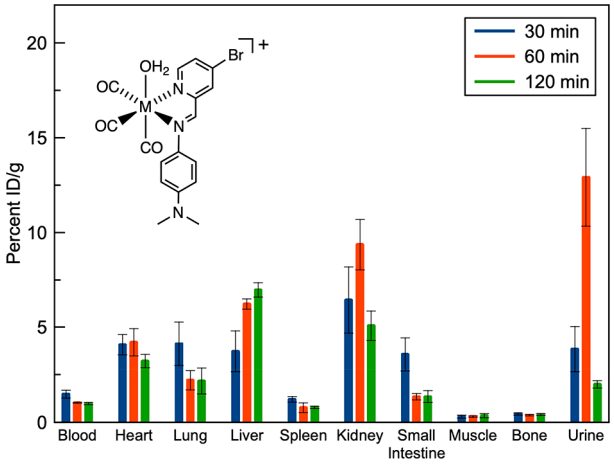

Figure 10. Biodistribution of ^{99m}**Tc-9D(H$_2$O)** in BALB/c mice detected using a γ counter, in which M is ^{99m}Tc, after 30 (blue), 60 (red), and 120 (green) min.

The urine (Figure 11) and blood (Figure S49, Supporting Information) of mice injected with ^{99m}**Tc-9D(H$_2$O)** were analyzed by HPLC coupled to a radiation detector. The resulting chromatograms reveal that this compound is relatively stable in vivo. The intact complex (t_r = 13.7 min) is observed in the urine at 30 and 60 min time points. Beyond 120 min, the majority of this compound has been cleared from the mice. In contrast, less radioactivity was detected in the blood overall. Hence, these samples were analyzed by extended γ counting of fractions that were isolated by HPLC. Analysis of the blood shows the intact compound to be present at 30 and 60 min postinjection with minimal activity observed at 120 min. Notably, the blood analysis reveals the presence of two more hydrophilic metabolites of an unknown nature. Further analysis on the nature of these species would aid in understanding the in vivo behavior of ^{99m}**Tc-9D(H$_2$O)**. Overall, the analysis of ^{99m}**Tc-9D(H$_2$O)** in both urine and blood samples show that an appreciable amount of this compound remains intact prior to and after renal and hepatic clearance.

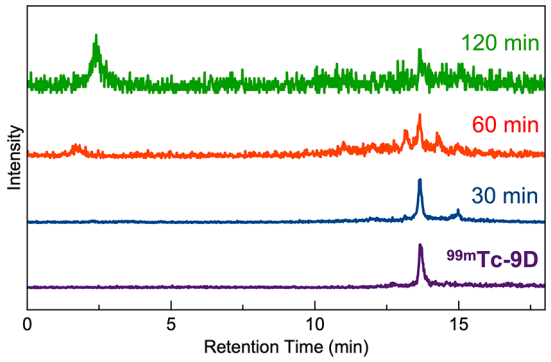

Figure 11. Direct HPLC traces of urine samples collected from mice treated with ^{99m}**Tc-9D(H$_2$O)** after 30 (blue), 60 (red), and 120 (green) minutes. Reference chromatogram of ^{99m}**Tc-9D(H$_2$O)** is shown (purple).

CONCLUSION

A library of rhenium tricarbonyl complexes was rapidly synthesized using a combinatorial approach in a microwave-assisted one-pot manner and subsequently screened against a panel of cancer cell lines. Lead compound identification from a single-dose screening at 10 μM revealed three complexes that were synthesized on a preparative scale and fully characterized. The three lead compounds, namely, **Re-9B**, **Re-9C**, and **Re-9D**, were tested for anticancer activity in ovarian cancer cell lines, and the most potent complex, **Re-9D**, was shown to lack cross-resistance with cisplatin and to induce cancer cell death via necrosis. Additionally, the ^{99m}Tc analogue of **Re-9D** bearing a water axial ligand, ^{99m}**Tc-9D(H$_2$O)**, showed a favorable clearance profile. The high metabolic stability of ^{99m}**Tc-9D(H$_2$O)** qualifies this compound and its corresponding rhenium analogue as promising structural entities for the development of anticancer agents. As demonstrated in this study, we have proved that the application of combinatorial synthesis enables the ability to rapidly obtain and screen a fairly large library of compounds, and it represents a valuable strategy for discovering new anticancer agents based on metal-containing complexes. Ongoing efforts are directed toward expanding the scope of this combinatorial synthesis to yield small libraries of complexes bearing different diimine and axial ligands. The discovery and application of these additional one-pot multi-component reactions will broaden the structural versatility of potential metal-based anticancer agents.

EXPERIMENTAL SECTION

Physical Measurements. Microwave-assisted synthesis was performed using a Kenmore microwave oven (1100 W, 120 V, 13 A). NMR samples were prepared in DMSO-d_6 and analyzed either on a 500 MHz Bruker AV 3HD spectrometer equipped with a broadband Prodigy cryoprobe or on an INOVA 400 MHz NMR spectrometer. ^{1}H NMR spectra were analyzed using MestReNova and referenced to the residual DMSO solvent peak at 2.50 ppm. Analytical RP-HPLC was performed using a Shimadzu LC20-AT HPLC equipped with an Ultra

DOI: 10.1021/acs.inorgchem.8b03552
Inorg. Chem. 2019, 58, 3895−3909

Aqueous C18 column, 100 Å, 5 μm, 250 mm × 4.6 mm (Restek) and an SPD-20AV UV−vis detector monitoring at 220 and 270 nm with a flow rate of 1 mL/min. Gradient elution began with 10% Solvent B in water containing 0.1% trifluoracetic acid (TFA) for 5 min followed by a linear gradient to 100% Solvent B over 20 min and then an additional 5 min of 100% Solvent B, where Solvent B is either MeOH or ACN. Samples were prepared for FTIR spectroscopy as KBr pellets and analyzed on a Thermo Nicolet Avatar 370 DTGS FTIR spectrometer. UV−vis spectra were acquired using an Agilent Cary 8454 UV−vis spectrophotometer. EA (CHN) was performed by Atlantic Microlab Inc. High-resolution mass spectra were recorded on an Exactive Orbitrap mass spectrometer in positive ESI mode (ThermoFisher Scientific). Absorbance and fluorescence signatures from cell viability assays were measured using a Biotek Synergy HT plate reader. Flow cytometry experiments were performed on a BD FACSAria Fusion flow cytometer. GFAAS was performed on a PerkinElmer PinAAcle 900Z AA spectrometer. ICP-MS was performed using an ELAN DRC-E ICP-MS equipped with an S-10 autosampler. Optical microscopy was performed using a VWR trinocular inverted microscope equipped with a V10 microscope camera and processed using Motic Images Plus 2.0 ML. Confocal fluorescence microscopy was performed by a Zeiss LSM 800 confocal laser scanning microscope equipped with 20× 0.8 NA and 40× 1.4 NA Plan Apochromat objectives, 405, 488, 561, and 640 nm solid-state lasers, and two GaAsP photomultiplier tube detectors.

Materials and Reagents. All reagents were purchased from commercial vendors. The lead rhenium complexes and the corresponding free ligands were synthesized according to literature methods with slight modifications.[38,39] All reactions were performed under ambient atmospheric conditions without any efforts to exclude oxygen or water. Solvents used were of ACS grade or higher.

Synthesis of Rhenium Compound Library. Stock solutions of starting reagents were prepared in DMSO. With the predetermined assignments for our combinatorial approach (Figure 1b), stock solutions were added to a 96-well plate resulting in 200 μL of 1 mM starting reagents in DMSO. The plate was then heated in a microwave for 3 min to yield 80 different rhenium complexes. Reaction progression and purity were determined using RP-HPLC in ACN and water. All complexes were used without further purification for the screening process.

Synthesis of 9B. *N,N*-Dimethyl-*p*-phenylenediamine (37 μL, 0.27 mmol) and 4-methylpicolinaldehyde (30 μL, 0.27 mmol) were heated at reflux in 5 mL of MeOH for 30 min. The solution was cooled to room temperature, and the solvent was removed under reduced pressure to obtain pure material as yellow-green powder. Yield: 63 mg (98%). ^{1}H NMR (500 MHz, DMSO-d_6): δ 8.60 (s, 1H), 8.51 (d, 1H), 7.95 (s, 1H), 7.34 (d, 2H), 7.28 (m, 1H), 6.76 (d, 2H), 2.95 (s, 6H). Anal. Calcd for **9B**·0.1H_2O ($C_{15}H_{17.2}N_3O_{0.1}$): C, 74.72; H, 7.19; N, 17.43. Found: C, 74.42; H, 7.13; N, 17.63%. ESI-MS (positive ion mode, MeOH): m/z 240.1489, calcd 240.1501 for $[M + H]^+$.

Synthesis of 9C. *N,N*-Dimethyl-*p*-phenylenediamine (37 μL, 0.27 mmol) and 4-chloropicolinaldehyde (38 mg, 0.27 mmol) were heated at reflux in 5 mL of MeOH for 30 min. The solution was cooled to room temperature, and the solvent was removed under reduced pressure to obtain pure material as a yellow-light green powder. Yield: 69 mg (99%). ^{1}H NMR (500 MHz, DMSO-d_6): δ 8.65 (s, 1H), 8.64 (d, 1H), 8.10 (d, 1H), 7.59 (dd, 1H), 7.40 (dt, 2H), 6.77 (dt, 2H), 2.97 (s, 6H). Anal. Calcd for **9C** ($C_{14}H_{14}ClN_3$): C, 64.74; H, 5.43; N, 16.18. Found: C, 64.58; H, 5.46; N, 16.02%. ESI-MS (positive ion mode, MeOH): m/z 260.0945, calcd 260.0955 for $[M + H]^+$.

Synthesis of 9D. *N,N*-Dimethyl-*p*-phenylenediamine (19.5 μL, 0.14 mmol) and 4-bromopicolinaldehyde (25 mg, 0.13 mmol) were heated at reflux in 5 mL of MeOH for 30 min. The solution was cooled to room temperature, and the solvent was removed under reduced pressure. The precipitate was recrystallized in 1:5 MeOH/Et_2O, vacuum-filtered, and washed with diethyl ether to obtain pure material as a yellow-brown powder. Yield: 33 mg (77%). ^{1}H NMR (500 MHz, DMSO-d_6): δ 8.63 (s, 1H), 8.54 (d, 1H), 8.25 (d, 1H), 7.71 (dd, 1H), 7.43 (dt, 2H), 6.79 (dt, 2H) 2.96 (s, 6H). Anal. Calcd for **9D** ($C_{14}H_{14}BrN_3$): C, 55.28; H, 4.64; N, 13.81. Found: C, 55.30; H, 4.63; N, 13.62%. ESI-MS (positive ion mode, MeOH): m/z 260.0945, calcd 260.0955 for $[M + H]^+$.

Synthesis of Re-9B. *N,N*-Dimethyl-*p*-phenylenediamine (19 μL, 0.14 mmol) and 4-methylpicolinaldehyde (15.7 μL, 0.14 mmol) were stirred in 3 mL of MeOH for 20 min. $Re(CO)_5Cl$ (50 mg, 0.14 mmol) was added to the reaction mixture and heated at reflux for 4 h. The solution containing red precipitate was cooled to room temperature and concentrated under reduced pressure to ∼0.5 mL, and 20 mL of diethyl ether was added to further precipitate the rhenium complex. The mixture was vacuum-filtered and washed with diethyl ether to obtain pure material as a bright red powder. Yield: 51 mg (68%). IR (KBr, ν(CO) cm^{-1}): 1880, 1907, 2016. ^{1}H NMR (500 MHz, DMSO-d_6): δ 9.12 (s, 1H), 8.84 (d, 1H), 8.10 (s, 1H), 7.60 (d, 1H), 7.47 (d, 2H), 6.83 (d, 2H), 3.00 (s, 6H), 2.54 (s, 3H). Anal. Calcd for **Re-9B** ($C_{18}H_{17}ClN_3O_3Re$): C, 39.67; H, 3.14; N, 7.71. Found: C, 39.93; H, 3.09; N, 7.83%. ESI-MS (positive ion mode, MeOH): m/z 588.0944, calcd 588.0967 for $[M-Cl + DMSO]^+$.

Synthesis of Re-9C. *N,N*-Dimethyl-*p*-phenylenediamine (19 μL, 0.14 mmol) and 4-chloropicolinaldehyde (20 mg, 0.14 mmol) were stirred in 3 mL of MeOH for 20 min. $Re(CO)_5Cl$ (50 mg, 0.14 mmol) was added to the reaction mixture and heated at reflux for 4 h. The solution containing red-purple precipitate was cooled to room temperature and concentrated under reduced pressure to ∼0.5 mL, and 20 mL diethyl ether was added to further precipitate the rhenium complex. The mixture was vacuum-filtered and washed with diethyl ether to obtain pure material as a shiny red-purple powder. Yield: 34 mg (44%). IR (KBr, ν(CO) cm^{-1}): 1856, 1930, 2018. ^{1}H NMR (500 MHz, DMSO-d_6): δ 9.13 (s, 1H), 8.95 (d, 1H), 8.40 (d, 1H), 7.87 (dd, 1H), 7.51 (dt, 2H), 6.87 (dt, 2H), 3.02 (s, 6H). Anal. Calcd for **Re-9C** ($C_{17}H_{14}Cl_2N_3O_3Re$): C, 36.11; H, 2.50; N, 7.43. Found: C, 36.32; H, 2.51; N, 7.26%. ESI-MS (positive ion mode, MeOH): m/z 608.0406, calcd 608.0421 for $[M-Cl + DMSO]^+$.

Synthesis of Re-9D. *N,N*-Dimethyl-*p*-phenylenediamine (19 μL, 0.14 mmol) and 4-bromopicolinaldehyde (26 mg, 0.14 mmol) were stirred in 3 mL of MeOH for 20 min. $Re(CO)_5Cl$ (50 mg, 0.14 mmol) was added to the reaction mixture and heated at reflux for 4 h. The solution containing dark red precipitate was cooled to room temperature, and the solvent was removed under vacuum. To the reaction flask was added 2 mL of tetrahydrofuran (THF) followed by the addition of 20 mL of diethyl ether. The sticky red material was filtered off and washed with ∼15 mL of THF. The filtrate was concentrated under reduced pressure to ∼0.5 mL, and 20 mL of diethyl ether was added to precipitate the rhenium complex. The mixture was vacuum-filtered and washed with diethyl ether to obtain the pure product as a red-purple powder. Yield: 28 mg (33%). IR (KBr, ν(CO) cm^{-1}): 1848, 1923, 2017. ^{1}H NMR (500 MHz, DMSO-d_6): δ 9.11 (s, 1H), 8.84 (d, 1H), 8.53 (d, 1H), 8.00 (dd, 1H), 7.50 (dt, 2H), 6.85 (dt, 2H), 3.02 (s, 6H). Anal. Calcd for **Re-9D** ($C_{17}H_{14}BrClN_3O_3Re$): C, 33.48; H, 2.31; N, 6.89. Found: C, 33.72; H, 2.23; N, 6.87%. ESI-MS (positive ion mode, MeOH): m/z 651.9894, calcd 651.9915 for $[M-Cl + DMSO]^+$.

Structure−Activity Relationship Determination. The log *P* values of the free ligands were calculated using the ALOGPS 2.1 program.[42,43] The Hammett constants were also compared and tabulated for each aldehyde and aniline.[44,45,48]

X-ray Crystallography. X-ray diffraction quality single crystals of **Re-9B** were obtained from DMSO upon standing, and single crystals of **Re-9C** and **Re-9D** were obtained through vapor diffusion of diethyl ether into THF. Low-temperature X-ray diffraction data were collected on a Rigaku XtaLAB Synergy diffractometer coupled to a Rigaku Hypix detector with Mo Kα radiation (λ = 0.710 73 Å) from a PhotonJet microfocus X-ray source at 100 K. The diffraction images were processed and scaled using the CrysAlisPro software.[102] The structures were solved using the Olex2 Software[103] through intrinsic phasing using SHELXT[104] and refined against F^2 on all data by full-matrix least-squares with SHELXL[105] following established refinement strategies.[106] All non-hydrogen atoms were refined anisotropically. All hydrogen atoms bound to carbon were included in the model at geometrically calculated positions and refined using a riding model. The isotropic displacement parameters of all hydrogen atoms were fixed to

DOI: 10.1021/acs.inorgchem.8b03552
Inorg. Chem. 2019, 58, 3895−3909

1.2 times the U_{eq} value of the atoms they are linked to (1.5 times for methyl groups). In the structures of **Re-9B** and **Re-9D**, the axial CO and Cl ligands are disordered over two locations and were modeled using the appropriate similarity restraints. The occupancy of the two parts were refined freely with the net sum occupancy set to 1. The carbon of the axial CO ligand in the structure of **Re-9C** was refined with the anisotropic displacement parameter equal to that of the equatorial CO carbon atoms using the EADP command in SHELXL. Details of the data quality and a summary of the residual values of the refinements are listed in Tables 1 and S4 (Supporting Information).

General Cell Culture. Cells were cultured as monolayers in a humidified incubator at 37 °C with 5% CO_2. The wild-type human ovarian cancer cell line A2780 and cisplatin-resistant A2780CP70 were obtained from the Cell Culture Facility of Fox Chase Cancer Center. The human cervical cancer (HeLa) and human embryonic kidney (HEK293) cells were obtained from the American Type Culture Collection. A2780 and A2780CP70 cells were cultured in Roswell Park Memorial Institute (RPMI) media containing 10% FBS; HeLa cells were cultured in Dulbecco's Modified Eagle Medium (DMEM) containing 10% FBS, and HEK293 cells were cultured in minimum essential media (MEM) containing 10% FBS. Cells were routinely passed at 80−90% confluency using 0.05% trypsin, 0.53 mM ethylenediaminetetraacetic acid (EDTA), 1× solution. Cell lines were tested monthly for contamination using the InvivoGen mycoplasma detection kit, PlasmoTest.

Cytotoxicity. Screening of the rhenium compound library was completed by first diluting stock solutions in Milli-Q water (18.2 MΩ·cm) to yield 100 μM solutions in 10% DMSO. These diluted solutions were screened against three cell lines: HeLa, A2780, and A2780CP70. Cells were seeded in 96-well plates at 4000 cells/well and allowed to adhere for 24 h. To each well was added 180 μL of growth media and 20 μL of the rhenium complexes (final concentrations at 10 μM, 1% DMSO), and then analyzed after 48 h using an MTT assay described below. Three independent experiments were conducted.

Dose-escalation studies were performed for the three lead compounds, free ligands, and starting materials. First, stock solutions of rhenium complexes, free ligands, and starting materials were prepared as 20 mM solutions in DMSO. Solutions for dose-dependent studies were prepared by first directly diluting stock solutions 1:100 in growth media (200 μM, 1% DMSO) and serially diluting 1:4 for further concentrations. Cells were seeded in a 96-well plate at a density of 4000 cells/well and allowed to adhere for 24 h. Growth media was removed, and the cells were dosed with 200 μL of compounds in a dose-dependent manner for 48 h, then analyzed using an MTT assay described below.

GSH dependence experiments were performed for **Re-9D**. First, the effects of increased levels of GSH were explored. A2780CP70 cells were seeded in 96-well plates at 4000 cells/well and allowed to adhere for 24 h. Growth media was removed, and 100 μL of GSH was then added in varying concentrations from 0 to 32 μM followed immediately by 100 μL of 200 μM **Re-9D** or 200 μM cisplatin in growth media for 48 h, then analyzed using an MTT assay described below.

In addition to determining the effects of cotreatment with GSH on anticancer activity, changes in cytotoxicity were also explored in samples with depleted levels of GSH using BSO. Solutions for dose-dependent studies were first prepared by first directly diluting stock solutions 1:100 in growth media (200 μM, 1% DMSO) and serially diluting 1:4 for further concentrations. A2780CP70 cells were seeded in 96-well plates at 4000 cells/well and allowed to adhere for 24 h. Growth media was then removed, and cells were treated with 100 μL of 10 mM of BSO for 24 h. The BSO solutions were replaced with 200 μL of cisplatin or **Re-9D** in varying concentrations and incubated for 48 h, then analyzed using an MTT assay described below.

MTT assays were performed following compound treatment by first replacing growth media with 200 μL MTT (1 mg/mL). Cells were incubated with the dye for 4 h, and growth media was removed to yield purple formazan crystals. The crystals were dissolved in 200 μL of DMSO containing 12% glycine buffer (0.1 M glycine, 0.1 M NaCl, pH 10.5). The absorbance was measured at 570 nm for each well using a Biotek Synergy HT plate reader. For dose-escalation studies, each plate contained six replicates per concentration, and at least three independent experiments were conducted with the same procedures. Data points were fit to the equation

$$y = E_{inf} + \frac{E_0 - E_{inf}}{1 + \left(\frac{D}{IC_{50}}\right)^{HS}}$$

where y is cell viability, E_{inf} is the viability at infinite drug concentration, E_0 is the viability at zero drug concentration, D is the drug concentration, IC_{50} is the 50% growth inhibitory concentration, and HS is the Hill slope.[55] E_0 was constrained to lie between 0.9 and 1.15. The compounds' IC_{50} values were determined by fitting the data and solving for these variables using the curve-fitting program MagicPlot Pro.

Tumor Spheroid Growth and Viability. Tumor spheroid models were prepared in agarose-coated 96-well plates. To begin making the agarose-coated plates, a solution of 0.5 g agarose in 40 mL of RPMI was autoclaved for 20 min at 120 °C. Immediately after autoclaving, 55 μL of agarose solution was pipetted into a 96-well plate. After they cooled to form a gel, the plates were stored in the dark in a sterile incubator at 37 °C until ready for use. In the agarose-coated 96-well plates, 100 μL of A2780 ovarian cancer cells were seeded at a density of 20 000 cells/well. The cells were allowed to form spheroids over a period of 3−5 d yielding diameters between 250 and 300 μm. Solutions for dose-dependent studies were prepared by first directly diluting stock solutions 1:100 in growth media (200 μM, 1% DMSO) and serially diluting 1:4 for further concentrations. To the tumor spheroid solutions were added 50 μL of cisplatin or **Re-9D** in varying concentrations. After incubation for 48 h, 30 μL of resazurin solution in Dulbecco's phosphate-buffered saline (DPBS; 0.15 mg/mL) was added to each well. Cells were incubated with the dye for 4 h, and then the fluorescence was read on a Biotek Synergy HT plate reader with excitation at 545/40 nm and emission at 590/25 nm. Each plate contained six replicates, and three independent experiments were completed.

Cellular Uptake and Organelle Isolation. A2780 or A2780CP70 ovarian cancer cells were plated in 100 mm × 20 mm tissue culture dishes and allowed to grow to 80% confluency. Growth media was then replaced with 6 mL of 10 μM **Re-9D** or 0.05% v/v DMSO as a negative control. After 24 h, the cells were washed with 3 mL of DPBS and harvested using trypsin. Cell lysates were then obtained for whole cell, nuclear, and mitochondrial samples using modified versions of previously described methods shown below.[80] The bicinchoninic acid (BCA) assay was used to determine protein content for lysate samples. The procedure for measuring protein content was previously described by the manufacturer.[107] In a 96-well plate, 25 μL of cell lysate was combined with 200 μL of working reagent and incubated for 30 min, and then the absorbance was measured at 562 nm. Protein concentrations were then extrapolated from a calibration curve using bovine serum albumin (BSA) standard dilutions. Samples were measured in triplicates.

Whole cell lysates were obtained by centrifuging harvested cells, washing with 1 mL of DPBS, lysing with 1 mL of 4% sodium dodecyl sulfate (SDS) lysis buffer (4% w/v SDS, 150 mM NaCl, 50 mM triethanolamine), and vortexing on the highest setting for 10 s. The supernatant was transferred to a clean tube. For GFAAS analysis, the lysates were analyzed without further sample preparation. For ICP-MS analysis, 750 μL of the lysate was diluted with an additional 750 μL of Milli-Q water and 5 mL of 70% HNO_3 followed by sonication for 30 min. After digestion, 3 mL of the resulting solution was diluted with 8 mL of Milli-Q water. The rhenium and platinum concentrations in each sample were determined using ICP-MS and GFAAS, respectively. Results were reported as the mass ratio of metal to protein (ng/μg) in each sample, in which protein content was determine using a BCA assay.

Nuclear lysate samples for ICP-MS were prepared from one 100 mm × 20 mm tissue culture dish, whereas samples for GFAAS were prepared from four dishes. The harvested cells were centrifuged and washed with 1 mL of DPBS then resuspended in 1 mL of hypotonic

DOI: 10.1021/acs.inorgchem.8b03552
Inorg. Chem. 2019, 58, 3895−3909

buffer (20 mM Tris-HCl, 10 mM NaCl, 3 mM $MgCl_2$, pH 7.4). After incubation on ice for 20 min, 50 μL of 10% w/v NP-40 was added, and the solution was vortexed on the highest setting for 10 s. After it was centrifuged at 3000*g* for 10 min, the pellet was resuspended in 1 mL of Milli-Q water and sonicated for 10 min. After it was lysed, 750 μL of the lysate was transferred to a clean tube. For GFAAS analysis, the lysate was analyzed without further sample preparation. For ICP-MS analysis, samples were further digested with an additional 750 μL of 2% HNO_3. The rhenium and platinum concentrations in each sample were determined using ICP-MS and GFAAS, respectively. Results were reported as the mass ratio of metal to protein (ng/μg) in each sample.

Mitochondrial lysate samples for ICP-MS were prepared from one 100 mm × 20 mm tissue culture dish, whereas samples for GFAAS were prepared from four dishes. The harvested cells were centrifuged, washed with 1 mL of DPBS, and then resuspended in 500 μL mitochondria extraction buffer (200 mM mannitol, 68 mM sucrose, 50 mM piperazine-*N*,*N*′-bis(2-ethanesulfonic acid) (PIPES), 50 mM KCl, 5 mM ethylene glycol-bis(β-aminoethyl ether)-*N*,*N*,*N*′,*N*′-tetraacetic acid (EGTA), 2 mM $MgCl_2$, 1 mM dithiothreitol, 1:500 v/v protease inhibitor cocktail) and incubated over ice for 20 min. The suspension was then homogenized by 35 passes through a 25 gauge needle and a 1 mL syringe. After centrifuging at 150 g for 5 min, the supernatant was transferred to a new microcentrifuge tube and centrifuged at 10 000*g* for 10 min. The resulting pellet was resuspended in 1 mL of Milli-Q water and sonicated for 10 min. To a 1.5 mL cryovial, 750 μL of the lysate was transferred to a clean tube. For GFAAS analysis, the lysate was analyzed without further sample preparation. For ICP-MS analysis, samples were further digested with an additional 750 μL of 2% HNO_3. The rhenium and platinum concentrations in each sample were determined using ICP-MS and GFAAS, respectively. Results were reported as the mass ratio of metal to protein (ng/μg) in each sample.

Flow Cytometry. Cell cycle analysis was conducted using A2780 cells, which were cultured in 100 mm × 20 mm tissue culture dishes and allowed to grow to 50% confluency. Cells were then dosed with varying concentrations of cisplatin or **Re-9D**. After incubation with compounds for 24 h, cells were harvested using trypsin and washed with 1 mL of DPBS. Cells were then fixed with 1 mL of 70% EtOH and stored at 4 °C until the day of analysis. The cells were washed twice with 1 mL of DPBS, resuspended in 200 μL of DPBS, and treated with 50 μL of RNase (100 μg/mL) and 20 μL of PI. After incubation for 30 min in the dark, 500 μL of DPBS was added, and samples were analyzed on a BD FACSAria Fusion flow cytometer.

The lead compound was evaluated for its ability to induce apoptosis using the annexin V−PI assay. A2780 cells were cultured in 25 cm^2 tissue culture flasks and grown to 80% confluency. Cells were then dosed with varying concentrations of **Re-9D** or cisplatin, and positive control cells were either heat-treated at 60 °C for 10 min or dosed with 80 μM etoposide. After incubation with compounds for 24 h, cells were harvested using trypsin and washed with 1 mL of DPBS. To the cell pellets were added 4 μL of PI (1 mg/mL) and 4 μL of annexin V-Alexa Fluor 488 followed by 100 μL of annexin binding buffer. After incubation for 15 min, an additional 400 μL of binding buffer was mixed into solution. Cells were then immediately analyzed on a BD FACSAria Fusion flow cytometer.

Live Cell Imaging. Brightfield time-lapse microscopy experiments were conducted with A2780CP70 ovarian cancer cells seeded at a density of 2.5 × 10^5 cells/well in six-well plates, which were allowed to adhere for 24 h. The growth media was then replaced with 1 mL of 60 μM **Re-9D**. The cells were immediately imaged using a VWR trinocular inverted microscope equipped with a V10 microscope camera and processed using Motic Images Plus 2.0 ML. Images were compiled and exported as a video file in iMovie.

Time-lapse confocal fluorescence microscopy experiments were conducted with A2780CP70 ovarian cancer cells seeded in 35 mm MatTek glass-bottomed culture dishes at a density of 2.5 × 10^5 cells/dish, which were allowed to adhere for 24 h. The growth media was then replaced with 1 mL of stock solution (60 μM **Re-9D**, 15 μg/mL PI). The cells were immediately imaged using a Zeiss LSM 800 confocal laser scanning microscope equipped with 20× 0.8 NA and 40× 1.4 NA Plan Apochromat objectives, 405, 488, 561, and 640 nm solid-state lasers, and two GaAsP photomultiplier tube detectors. Samples were excited at 405 and 561 nm, and the emission wavelengths measured were 410−550 and 590−700 nm. Images were then processed using FIJI/ImageJ.

Radiolabeling Protocol for ^{99m}Tc. RadioHPLC analysis was performed using a Shimadzu HPLC-20AR equipped with a binary gradient pump, UV−vis detector, autoinjector, and Laura radiodetector. UV absorption was recorded at 254 and 280 nm, samples were analyzed using a C18 column (Phenomenex Gemini C18, 150 mm × 4.60 mm), 0.8 mL/min flow, with mobile phase method 1: Solvent A: 50 mM tetraethylammonium phosphate (TEAP, pH 2) in water, Solvent B: MeOH. 0−2 min: 5% B; 2−14 min: 5−95% B; 14−19 min: 95% B; 19−19.5 min: 95−5% B; 19.5−25 min: 5% B. The $[Re(\mathbf{9D})(CO)_3(H_2O)]^+$ complex (**Re-9D(H$_2$O)**) was synthesized by treatment of **Re-9D** with 10 equiv of Ag(TFA) at 50 °C. ^{99m}Tc-labeling involved the initial synthesis of technetium tricarbonyl precursor $[^{99m}Tc(H_2O)_3(CO)_3]^+$. Sodium pertechnetate, $Na[^{99m}TcO_4]$, was eluted from a ^{99} Mo/^{99m}Tc sterile generator as a 1.0 mL saline solution (0.9% v/v) and provided by Triad Isotopes (Triad Isotopes). The radioactive solution was added to a sealed vial containing boranocarbonate (4 mg), sodium tartrate (7 mg), and sodium borate decahydrate (7 mg), and carbonylation was performed under heating for 40 min at 100 °C using an oil bath. The solution was cooled to room temperature. A separate solution of ligand **9D** (100 μM in MeOH) was prepared. To the aqueous $[^{99m}Tc(H_2O)_3(CO)_3]^+$ solution (1 mL) was added 1 M HCl (150−180 μL), to adjust the pH to 7. A 500 μL aliquot was removed and mixed with ligand stock solution (100 μL), and the mixture was heated to 50 °C for 30 min under vigorous stirring in a sealed reaction vessel. The reaction was analyzed using method 1 to monitor progress and radiochemical yield of the reaction. Preparative purification of complexes was performed using large-volume HPLC injections followed by manual collection of the assigned product peak. *Retention times (all reported using method 1):* **^{99m}Tc-9D(H$_2$O)**: 13.65 min. **Re-9D(H$_2$O)**: 13.63 min. **Re-9D**: 14.97 min. Radiochemical yield: 48%. Radiochemical purity after HPLC purification: 99%.

Biodistribution and Metabolite Analysis. All animal experiments were conducted according to the guidelines of the Institutional Animal Care and Use Committee (IACUC) of Stony Brook University at the Department of Laboratory Animal Resources (DLAR), Stony Brook Medicine. Female BALB/c mice (six weeks old, Taconic Biosciences) were intravenously injected with 90−160 μCi of **^{99m}Tc-9D(H$_2$O)**. Complex **Re-9D** exhibited poor solubility in various biocompatible solvents, and no significant dose could be administered intravenously. Mice were sacrificed at 30, 60, and 120 min post injection (n = 3, 4 per time point). The following organs were harvested and collected: blood (obtained via cardiac puncture), heart, liver, lung, kidney, spleen, small intestine, muscle (thigh), bone (femur), urine. Urine was collected for metabolite analysis via bladder puncture. Radioactivity was counted using a γ counter. Radioactivity associated with each organ was expressed as percent injected dose per gram (% ID/g). Metabolite analysis of blood and urine was performed for all time points, with all urine metabolite time points yielding directly discernible HPLC chromatograms, whereas blood metabolite time points were obtained from fractioned collection of HPLC eluent and subsequent reconstruction of the chromatogram (Figure S49, Supporting Information).

■ ASSOCIATED CONTENT

Supporting Information

The Supporting Information is available free of charge on the ACS Publications website at DOI: 10.1021/acs.inorgchem.8b03552.

Complex characterization data including calculated log *P* values, Hammett parameter constants, NMR, IR, UV−vis spectra, HPLC chromatograms, crystallographic data, and dose−response curves. Additional biological studies including combinatorial screening, flow cytometry data, time-lapse microscopy results, and in vivo studies. (PDF)

DOI: 10.1021/acs.inorgchem.8b03552
Inorg. Chem. 2019, 58, 3895−3909

Changes in cellular morphology (AVI)
Cellular autofluorescence and PI (AVI)

Accession Codes

CCDC 1885033−1885035 contain the supplementary crystallographic data for this paper. These data can be obtained free of charge via www.ccdc.cam.ac.uk/data_request/cif, or by emailing data_request@ccdc.cam.ac.uk, or by contacting The Cambridge Crystallographic Data Centre, 12 Union Road, Cambridge CB2 1EZ, UK; fax: +44 1223 336033.

AUTHOR INFORMATION

Corresponding Author

*E-mail: jjw275@cornell.edu.

ORCID

Chilaluck C. Konkankit: 0000-0002-3253-0132
Samantha N. MacMillan: 0000-0001-6516-1823
Eszter Boros: 0000-0002-4186-6586
Justin J. Wilson: 0000-0002-4086-7982

Notes

The authors declare no competing financial interest.

ACKNOWLEDGMENTS

Work in our laboratory is supported by Cornell Univ. and by the Office of the Assistant Secretary of Defense for Health Affairs through the Ovarian Cancer Research Program under Award No. W81XWH-17-1-0097. The content is solely the responsibility of the authors and does not necessarily represent the official views of the Office of the Assistant Secretary of Defense for Health Affairs. This work has made use of the NMR facilities at Cornell Univ., which are supported by the National Science Foundation under Award No. CHE-1531632. S. Davalos is thanked for assistance with preparing the artwork associated with this manuscript. S. C. Marker is thanked for assistance with time-lapse confocal fluorescence microscopy studies. D. A. Driscoll is thanked for assistance with ICP-MS studies.

REFERENCES

(1) Henderson, J. T.; Webber, E. M.; Sawaya, G. F. Screening for Ovarian Cancer. *JAMA, J. Am. Med. Assoc.* **2018**, *319*, 595−606.
(2) Matulonis, U. A.; Sood, A. K.; Fallowfield, L.; Howitt, B. E.; Sehouli, J.; Karlan, B. Y. Ovarian Cancer. *Nat. Rev. Dis. Primers* **2016**, *2*, 1−22.
(3) Ushijima, K. Treatment for Recurrent Ovarian Cancer−At First Relapse. *J. Oncol.* **2010**, *2010*, 1−7.
(4) Tomao, F.; Marchetti, C.; Romito, A.; Di Pinto, A.; Di Donato, V.; Capri, O.; Palaia, I.; Monti, M.; Muzii, L.; Panici, P. B. Overcoming Platinum Resistance in Ovarian Cancer Treatment: From Clinical Practice to Emerging Chemical Therapies. *Expert Opin. Pharmacother.* **2017**, *18*, 1443−1455.
(5) Rocha, C. R. R.; Silva, M. M.; Quinet, A.; Cabral-Neto, J. B.; Menck, C. F. M. DNA Repair Pathways and Cisplatin Resistance: An Intimate Relationship. *Clinics* **2018**, *73*, No. e478s.
(6) Bowden, N. A. Nucleotide Excision Repair: Why Is It Not Used to Predict Response to Platinum-Based Chemotherapy? *Cancer Lett.* **2014**, *346*, 163−171.
(7) Martin, L. P.; Hamilton, T. C.; Schilder, R. J. Platinum Resistance: The Role of DNA Repair Pathways. *Clin. Cancer Res.* **2008**, *14*, 1291−1295.
(8) Godwin, A. K.; Meister, A.; O'Dwyer, P. J.; Huang, C. S.; Hamilton, T. C.; Anderson, M. E. High Resistance to Cisplatin in Human Ovarian Cancer Cell Lines Is Associated with Marked Increase of Glutathione Synthesis. *Proc. Natl. Acad. Sci. U. S. A.* **1992**, *89*, 3070−3074.
(9) Cepeda, V.; Fuertes, M. A.; Castilla, J.; Alonso, C.; Quevedo, C.; Pérez, J. M. Biochemical Mechanisms of Cisplatin Cytotoxicity. *Anti-Cancer Agents Med. Chem.* **2007**, *7*, 3−18.
(10) Estrela, J. M.; Ortega, A.; Obrador, E. Glutathione in Cancer Biology and Therapy. *Crit. Rev. Clin. Lab. Sci.* **2006**, *43*, 143−181.
(11) Ortega, A. L.; Mena, S.; Estrela, J. M. Glutathione in Cancer Cell Death. *Cancers* **2011**, *3*, 1285−1310.
(12) Ott, I.; Gust, R. Non Platinum Metal Complexes as Anti-Cancer Drugs. *Arch. Pharm.* **2007**, *340*, 117−126.
(13) Alessio, E.; Mestroni, G.; Bergamo, A.; Sava, G. Ruthenium Antimetastatic Agents. *Curr. Trends Med. Chem.* **2004**, *4*, 1525−1535.
(14) Rademaker-Lakhai, J. M.; van den Bongard, D.; Pluim, D.; Beijnen, J. H.; Schellens, J. H. M. A Phase I and Pharmacological Study with Imidazolium-*Trans*-DMSO-Imidazole-Tetrachlororuthenate, a Novel Ruthenium Anticancer Agent. *Clin. Cancer Res.* **2004**, *10*, 3717−3727.
(15) Hartinger, C. G.; Zorbas-Seifried, S.; Jakupec, M. A.; Kynast, B.; Zorbas, H.; Keppler, B. K. From Bench to Bedside − Preclinical and Early Clinical Development of the Anticancer Agent Indazolium *Trans*-[Tetrachlorobis(1*H*-Indazole)Ruthenate(III)] (KP1019 or FFC14A). *J. Inorg. Biochem.* **2006**, *100*, 891−904.
(16) Galanski, M.; Arion, V. B.; Jakupec, M. A.; Keppler, B. K. Recent Developments in the Field of Tumor-Inhibiting Metal Complexes. *Curr. Pharm. Des.* **2003**, *9*, 2078−2089.
(17) Gasser, G.; Ott, I.; Metzler-Nolte, N. Organometallic Anticancer Compounds. *J. Med. Chem.* **2011**, *54*, 3−25.
(18) Konkankit, C. C.; Marker, S. C.; Knopf, K. M.; Wilson, J. J. Anticancer Activity of Complexes of the Third Row Transition Metals, Rhenium, Osmium, and Iridium. *Dalton Trans.* **2018**, *47*, 9934−9974.
(19) Leonidova, A.; Gasser, G. Underestimated Potential of Organometallic Rhenium Complexes as Anticancer Agents. *ACS Chem. Biol.* **2014**, *9*, 2180−2193.
(20) Lee, L. C.-C.; Leung, K.-K.; Lo, K. K.-W. Recent Development of Luminescent Rhenium(I) Tricarbonyl Polypyridine Complexes as Cellular Imaging Reagents, Anticancer Drugs, and Antibacterial Agents. *Dalton Trans.* **2017**, *46*, 16357−16380.
(21) Jürgens, S.; Herrmann, W. A.; Kühn, F. E. Rhenium and Technetium Based Radiopharmaceuticals: Development and Recent Advances. *J. Organomet. Chem.* **2014**, *751*, 83−89.
(22) Knopf, K. M.; Murphy, B. L.; MacMillan, S. N.; Baskin, J. M.; Barr, M. P.; Boros, E.; Wilson, J. J. In Vitro Anticancer Activity and in Vivo Biodistribution of Rhenium(I) Tricarbonyl Aqua Complexes. *J. Am. Chem. Soc.* **2017**, *139*, 14302−14314.
(23) Marker, S. C.; MacMillan, S. N.; Zipfel, W. R.; Li, Z.; Ford, P. C.; Wilson, J. J. Photoactivated in Vitro Anticancer Activity of Rhenium(I) Tricarbonyl Complexes Bearing Water-Soluble Phosphines. *Inorg. Chem.* **2018**, *57*, 1311−1331.
(24) Akbar, M. U.; Ahmad, M. R.; Shaheen, A.; Mushtaq, S. A Review on Evaluation of Technetium-99m Labeled Radiopharmaceuticals. *J. Radioanal. Nucl. Chem.* **2016**, *310*, 477−493.
(25) Francis, M. B.; Finney, N. S.; Jacobsen, E. N. Combinatorial Approach to the Discovery of Novel Coordination Complexes. *J. Am. Chem. Soc.* **1996**, *118*, 8983−8984.
(26) Liu, R.; Li, X.; Lam, K. S. Combinatorial Chemistry in Drug Discovery. *Curr. Opin. Chem. Biol.* **2017**, *38*, 117−126.
(27) Shaikh, S. M.; Nalawade; Shete, A. S.; Doijad, R. C. A Review on Combinatorial Chemistry. *Res. Rev.: J. Chem.* **2017**, *6*, 14−26.
(28) Pandeya, S. N.; Thakhar, D. Combinatorial Chemistry: A Novel Method in Drug Discovery and Its Application. *Indian J. Chem.* **2005**, *44B*, 335−348.
(29) Maehr, H. Combinatorial Chemistry in Drug Research from a New Vantage Point. *Bioorg. Med. Chem.* **1997**, *5*, 473−491.
(30) Chow, M. J.; Licona, C.; Wong, D. Y. Q.; Pastorin, G.; Gaiddon, C.; Ang, W. H. Discovery and Investigation of Anticancer Ruthenium−Arene Schiff-Base Complexes via Water-Promoted Combinatorial Three-Component Assembly. *J. Med. Chem.* **2014**, *57*, 6043−6059.
(31) Chow, M. J.; Alfiean, M.; Pastorin, G.; Gaiddon, C.; Ang, W. H. Apoptosis-Independent Organoruthenium Anticancer Complexes

DOI: 10.1021/acs.inorgchem.8b03552
Inorg. Chem. 2019, 58, 3895−3909

That Overcome Multidrug Resistance: Self-Assembly and Phenotypic Screening Strategies. *Chem. Sci.* **2017**, *8*, 3641−3649.
(32) Ziegler, C. J.; Silverman, A. P.; Lippard, S. J. High-Throughput Synthesis and Screening of Platinum Drug Candidates. *JBIC, J. Biol. Inorg. Chem.* **2000**, *5*, 774−783.
(33) Robillard, M. S.; Bacac, M.; van den Elst, H.; Flamigni, A.; van der Marel, G. A.; van boom, J. H.; Reedijk, J. Automated Parallel Solid-Phase Synthesis and Anticancer Screening of a Library of Peptide-Tethered Platinum(II) Complexes. *J. Comb. Chem.* **2003**, *5*, 821−825.
(34) van Zutphen, S.; Stone, E. A.; van Rijt, S.; Robillard, M. S.; van der Marel, G. A.; Overkleeft, H. S.; den Dulk, H.; Brouwer, J.; Reedijk, J. Combinatorial Discovery of New Asymmetric *Cis* Platinum Anticancer Complexes Is Made Possible with Solid-Phase Synthetic Methods. *J. Inorg. Biochem.* **2005**, *99*, 2032−2038.
(35) Wachter, E.; Moyá, D.; Glazer, E. C. Combining a Ru(II) "Building Block" and Rapid Screening Approach to Identify DNA Structure-Selective "Light Switch" Compounds. *ACS Comb. Sci.* **2017**, *19*, 85−95.
(36) Mulcahy, S. P.; Gründler, K.; Frias, C.; Wagner, L.; Prokop, A.; Meggers, E. Discovery of a Strongly Apoptotic Ruthenium Complex through Combinatorial Coordination Chemistry. *Dalton Trans.* **2010**, *39*, 8177−8182.
(37) Ding, S.; Bierbach, U. Linker Design for the Modular Assembly of Multifunctional and Targeted Platinum(II)-Containing Anticancer Agents. *Dalton Trans.* **2016**, *45*, 13104−13113.
(38) Hasheminasab, A.; Engle, J. T.; Bass, J.; Herrick, R. S.; Ziegler, C. J. The Synthesis of Dimeric Re^{I}−Phenylenediimine Conjugates: Spectroscopic and Electrochemical Studies. *Eur. J. Inorg. Chem.* **2014**, *2014*, 2643−2652.
(39) Hasheminasab, A.; Wang, L.; Dawadi, M. B.; Bass, J.; Herrick, R. S.; Rack, J. J.; Ziegler, C. J. Induction of *E/Z* Isomerization in a Pendant Metal-Bound Azobenzene: A Synthetic, Spectroscopic and Theoretical Study. *Dalton Trans.* **2015**, *44*, 15400−15403.
(40) Yam, V. W.-W.; Wong, K. M.-C.; Lee, V. W.-M.; Lo, K. K.-W.; Cheung, K.-K. Synthesis, Photophysics, Ion-Binding Studies, and Structural Characterization of Organometallic Rhenium(I) Crown Complexes. *Organometallics* **1995**, *14*, 4034−4036.
(41) Dominey, R. N.; Hauser, B.; Hubbard, J.; Dunham, J. Structural, Spectral, and Charge-Transfer Properties of $ClRe(CO)_3$(2-PP) [2-PP = *N*-(2-Pyridinylmethylene)Phenylamine] and $ClRe(CO)_3$(2-PC) [2-PC = *N*-(2-Pyridinylmethylene)Cyclohexylamine]. *Inorg. Chem.* **1991**, *30*, 4754−4758.
(42) Tetko, I. V.; Bruneau, P. Application of ALOGPS to Predict 1-Octanol/Water Distribution Coefficients, Log*P*, and Log*D*, of AstraZeneca In-House Database. *J. Pharm. Sci.* **2004**, *93*, 3103−3110.
(43) Tetko, I. V.; Tanchuk, V. Y. Application of Associative Neural Networks for Prediction of Lipophilicity in ALOGPS 2.1 Program. *J. Chem. Inf. Model.* **2002**, *42*, 1136−1145.
(44) McDaniel, D. H.; Brown, H. C. An Extended Table of Hammett Substituent Constants Based on the Ionization of Substituted Benzoic Acids. *J. Org. Chem.* **1958**, *23*, 420−427.
(45) Santiago, C. B.; Milo, A.; Sigman, M. S. Developing a Modern Approach to Account for Steric Effects in Hammett-Type Correlations. *J. Am. Chem. Soc.* **2016**, *138*, 13424−13430.
(46) Merillas, B.; Cuéllar, E.; Diez-Varga, A.; Asensio-Bartolomé, M.; García-Herbosa, G.; Torroba, T.; Martín-Alvarez, J. M.; Miguel, D.; Villafañe, F. Whole Microwave Syntheses of Pyridylpyrazole and of Re and Ru Luminescent Pyridylpyrazole Complexes. *Inorg. Chim. Acta* **2019**, *484*, 1−7.
(47) Mosmann, T. Rapid Colorimetric Assay for Cellular Growth and Survival: Application to Proliferation and Cytotoxicity Assays. *J. Immunol. Methods* **1983**, *65*, 55−63.
(48) Hansch, C.; Leo, A.; Taft, R. W. A Survey of Hammett Substituent Constants and Resonance and Field Parameters. *Chem. Rev.* **1991**, *91*, 165−195.
(49) Kaplanis, M.; Stamatakis, G.; Papakonstantinou, V. D.; Paravatou-Petsotas, M.; Demopoulos, C. A.; Mitsopoulou, C. A. Re(I) Tricarbonyl Complex of 1,10-Phenanthroline-5,6-Dione: DNA Binding, Cytotoxicity, Anti-Infl Ammatory and Anti-Coagulant Effects towards Platelet Activating Factor. *J. Inorg. Biochem.* **2014**, *135*, 1−9.
(50) Chou, T.-C. Derivation and Properties of Michaelis−Menten Type and Hill Type Equations for Reference Ligands. *J. Theor. Biol.* **1976**, *59*, 253−276.
(51) Hill, A. The Possible Effects of the Aggregation of the Molecules of Haemoglobin on Its Dissociation Curves. *J. Physiol.* **1910**, *53*, 1689−1699.
(52) Shoichet, B. K. Interpreting Steep Dose-Response Curves in Early Inhibitor Discovery. *J. Med. Chem.* **2006**, *49*, 7274−7277.
(53) Shen, L.; Peterson, S.; Sedaghat, A. R.; McMahon, M. A.; Callender, M.; Zhang, H.; Zhou, Y.; Pitt, E.; Anderson, K. S.; Acosta, E. P.; Siliciano, R. F. Dose-Response Curve Slope Sets Class-Specific Limits on Inhibitory Potential of Anti-HIV Drugs. *Nat. Med.* **2008**, *14*, 762−766.
(54) Sampah, M. E. S.; Shen, L.; Jilek, B. L.; Siliciano, R. F. Dose-Response Curve Slope Is a Missing Dimension in the Analysis of HIV-1 Drug Resistance. *Proc. Natl. Acad. Sci. U. S. A.* **2011**, *108*, 7613−7618.
(55) Fallahi-Sichani, M.; Honarnejad, S.; Heiser, L. M.; Gray, J. W.; Sorger, P. K. Metrics Other than Potency Reveal Systematic Variation in Responses to Cancer Drugs. *Nat. Chem. Biol.* **2013**, *9*, 708−714.
(56) Abbott, A. Biology's New Dimension. *Nature* **2003**, *424*, 870−872.
(57) Friedrich, J.; Seidel, C.; Ebner, R.; Kunz-Schughart, L. A. Spheroid-Based Drug Screen: Considerations and Practical Approach. *Nat. Protoc.* **2009**, *4*, 309−324.
(58) Zanoni, M.; Piccinini, F.; Arienti, C.; Zamagni, A.; Santi, S.; Polico, R.; Bevilacqua, A.; Tesei, A. 3D Tumor Spheroid Models for *in Vitro* Therapeutic Screening: A Systematic Approach to Enhance the Biological Relevance of Data Obtained. *Sci. Rep.* **2016**, *6*, 1−11.
(59) Parsons, B. D.; Schindler, A.; Evans, D. H.; Foley, E. A Direct Phenotypic Comparison of siRNA Pools and Multiple Individual Duplexes in a Functional Assay. *PLoS One* **2009**, *4*, No. e8471.
(60) Ivanov, D. P.; Parker, T. L.; Walker, D. A.; Alexander, C.; Ashford, M. B.; Gellert, P. R.; Garnett, M. C. Multiplexing Spheroid Volume, Resazurin and Acid Phosphatase Viability Assays for High-Throughput Screening of Tumour Spheroids and Stem Cell Neurospheres. *PLoS One* **2014**, *9*, No. e103817.
(61) Walzl, A.; Unger, C.; Kramer, N.; Unterleuthner, D.; Scherzer, M.; Hengstschläger, M.; Schwanzer-Pfeiffer, D.; Dolznig, H. The Resazurin Reduction Assay Can Distinguish Cytotoxic from Cytostatic Compounds in Spheroid Screening Assays. *J. Biomol. Screening* **2014**, *19*, 1047−1059.
(62) Tanenbaum, L. M.; Mantzavinou, A.; Subramanyam, K. S.; del Carmen, M. G.; Cima, M. J. Ovarian Cancer Spheroid Shrinkage Following Continuous Exposure to Cisplatin Is a Function of Spheroid Diameter. *Gynecol. Oncol.* **2017**, *146*, 161−169.
(63) Balendiran, G. K.; Dabur, R.; Fraser, D. The Role of Glutathione in Cancer. *Cell Biochem. Funct.* **2004**, *22*, 343−352.
(64) Romero-Canelón, I.; Sadler, P. J. Next-Generation Metal Anticancer Complexes: Multitargeting via Redox Modulation. *Inorg. Chem.* **2013**, *52*, 12276−12291.
(65) Fu, Y.; Habtemariam, A.; Pizarro, A. M.; van Rijt, S. H.; Healey, D. J.; Cooper, P. A.; Shnyder, S. D.; Clarkson, G. J.; Sadler, P. J. Organometallic Osmium Arene Complexes with Potent Cancer Cell Cytotoxicity. *J. Med. Chem.* **2010**, *53*, 8192−8196.
(66) Howerton, B. S.; Heidary, D. K.; Glazer, E. C. Strained Ruthenium Complexes Are Potent Light-Activated Anticancer Agents. *J. Am. Chem. Soc.* **2012**, *134*, 8324−8327.
(67) Fu, Y.; Romero, M. J.; Habtemariam, A.; Snowden, M. E.; Song, L.; Clarkson, G. J.; Qamar, B.; Pizarro, A. M.; Unwin, P. R.; Sadler, P. J. The Contrasting Chemical Reactivity of Potent Isoelectronic Iminopyridine and Azopyridine Osmium(II) Arene Anticancer Complexes. *Chem. Sci.* **2012**, *3*, 2485−2494.
(68) Bailey, H. H. L-S,R-Buthionine Sulfoximine: Historical Development and Clinical Issues. *Chem.-Biol. Interact.* **1998**, *111*−*112*, 239−254.

DOI: 10.1021/acs.inorgchem.8b03552
Inorg. Chem. 2019, 58, 3895−3909

(69) Griffith, O. W.; Meister, A. Potent and Specific Inhibition of Glutathione Synthesis by Buthionine Sulfoximine (*S-n*-Butyl Homocysteine Sulfoximine). *J. Biol. Chem.* **1979**, *254*, 7558−7560.
(70) Griffith, O. W. Mechanism of Action, Metabolism, and Toxicity of Buthionine Sulfoximine and Its Higher Homologs, Potent Inhibitors of Glutathione Synthesis. *J. Biol. Chem.* **1982**, *257*, 13704−13712.
(71) Shnyder, S. D.; Fu, Y.; Habtemariam, A.; van Rijt, S. H.; Cooper, P. A.; Loadman, P. M.; Sadler, P. J. Anti-Colorectal Cancer Activity of an Organometallic Osmium Arene Azopyridine Complex. *MedChemComm* **2011**, *2*, 666−668.
(72) Li, Q.; Yin, X.; Wang, W.; Zhan, M.; Zhao, B.; Hou, Z.; Wang, J. The Effects of Buthionine Sulfoximine on the Proliferation and Apoptosis of Biliary Tract Cancer Cells Induced by Cisplatin and Gemcitabine. *Oncol. Lett.* **2016**, *11*, 474−480.
(73) Loh, S. Y.; Mistry, P.; Kelland, L. R.; Abel, G.; Harrap, K. R. Reduced Drug Accumulation as a Major Mechanism of Acquired Resistance to Cisplatin in a Human Ovarian Carcinoma Cell Line: Circumvention Studies Using Novel Platinum (II) and (IV) Ammine/Amine Complexes. *Br. J. Cancer* **1992**, *66*, 1109−1115.
(74) King, A. P.; Gellineau, H. A.; Ahn, J.-E.; MacMillan, S. N.; Wilson, J. J. Bis(Thiosemicarbazone) Complexes of Cobalt(III). Synthesis, Characterization, and Anticancer Potential. *Inorg. Chem.* **2017**, *56*, 6609−6623.
(75) Ghezzi, A.; Aceto, M.; Cassino, C.; Gabano, E.; Osella, D. Uptake of Antitumor Platinum(II)-Complexes by Cancer Cells, Assayed by Inductively Coupled Plasma Mass Spectrometry (ICP-MS). *J. Inorg. Biochem.* **2004**, *98*, 73−78.
(76) Kirin, S. I.; Ott, I.; Gust, R.; Mier, W.; Weyhermüller, T.; Metzler-Nolte, N. Cellular Uptake Quantification of Metalated Peptide and Peptide Nucleic Acid Bioconjugates by Atomic Absorption Spectroscopy. *Angew. Chem., Int. Ed.* **2008**, *47*, 955−959.
(77) Spreckelmeyer, S.; van der Zee, M.; Bertrand, B.; Bodio, E.; Stürup, S.; Casini, A. Relevance of Copper and Organic Cation Transporters in the Activity and Transport Mechanisms of an Anticancer Cyclometallated Gold(III) Compound in Comparison to Cisplatin. *Front. Chem.* **2018**, *6*, 1−15.
(78) Hostachy, S.; Policar, C.; Delsuc, N. Re(I) Carbonyl Complexes: Multimodal Platforms for Inorganic Chemical Biology. *Coord. Chem. Rev.* **2017**, *351*, 172−188.
(79) Clède, S.; Policar, C. Metal-Carbonyl Units for Vibrational and Luminescence Imaging: Towards Multimodality. *Chem. - Eur. J.* **2015**, *21*, 942−958.
(80) Komor, A. C.; Schneider, C. J.; Weidmann, A. G.; Barton, J. K. Cell-Selective Biological Activity of Rhodium Metalloinsertors Correlates with Subcellular Localization. *J. Am. Chem. Soc.* **2012**, *134*, 19223−19233.
(81) Groessl, M.; Zava, O.; Dyson, P. J. Cellular Uptake and Subcellular Distribution of Ruthenium-Based Metallodrugs under Clinical Investigation *versus* Cisplatin. *Metallomics* **2011**, *3*, 591−599.
(82) Sherr, C. J.; Bartek, J. Cell Cycle−Targeted Cancer Therapies. *Annu. Rev. Cancer Biol.* **2017**, *1*, 41−57.
(83) Dasari, S.; Tchounwou, P. B. Cisplatin in Cancer Therapy: Molecular Mechanisms of Action. *Eur. J. Pharmacol.* **2014**, *740*, 364−378.
(84) Zhang, D.; Piao, H.-L.; Li, Y.-H.; Qiu, Q.; Li, D.-J.; Du, M.-R.; Tsang, B. K. Inhibition of AKT Sensitizes Chemoresistant Ovarian Cancer Cells to Cisplatin by Abrogating S and G2/M Arrest. *Exp. Mol. Pathol.* **2016**, *100*, 506−513.
(85) Darzynkiewicz, Z. Critical Aspects in Analysis of Cellular DNA Content. *Curr. Protoc. Cytom.* **2011**, *56*, 7.2.1−7.2.8.
(86) Vaisman, A.; Varchenko, M.; Said, I.; Chaney, S. G. Cell Cycle Changes Associated With Formation of Pt-DNA Adducts in Human Ovarian Carcinoma Cells With Different Cisplatin Sensitivity. *Cytometry* **1997**, *27*, 54−64.
(87) Zhang, J.; Dai, Q.; Park, D.; Deng, X. Targeting DNA Replication Stress for Cancer Therapy. *Genes* **2016**, *7*, 51−66.
(88) Leventis, P. A.; Grinstein, S. The Distribution and Function of Phosphatidylserine in Cellular Membranes. *Annu. Rev. Biophys.* **2010**, *39*, 407−427.
(89) van Engeland, M.; Nieland, L. J. W.; Ramaekers, F. C. S.; Schutte, B.; Reutelingsperger, C. P. M. Annexin V-Affinity Assay: A Review on an Apoptosis Detection System Based on Phosphatidylserine Exposure. *Cytometry* **1998**, *31*, 1−9.
(90) Montecucco, A.; Zanetta, F.; Biamonti, G. Molecular Mechanisms of Etoposide. *EXCLI Journal* **2015**, *14*, 95−108.
(91) Nagata, S. Apoptosis and Clearance of Apoptotic Cells. *Annu. Rev. Immunol.* **2018**, *36*, 489−517.
(92) Berghe, T. V.; Vanlangenakker, N.; Parthoens, E.; Deckers, W.; Devos, M.; Festjens, N.; Guerin, C. J.; Brunk, U. T.; Declercq, W.; Vandenabeele, P. Necroptosis, Necrosis and Secondary Necrosis Converge on Similar Cellular Disintegration Features. *Cell Death Differ.* **2010**, *17*, 922−930.
(93) Bastian, A.; Thorpe, J. E.; Disch, B. C.; Bailey-Downs, L. C.; Gangjee, A.; Devambatla, R. K. V.; Henthorn, J.; Humphries, K. M.; Vadvalkar, S. S.; Ihnat, M. A. A Small Molecule with Anticancer and Antimetastatic Activities Induces Rapid Mitochondrial-Associated Necrosis in Breast Cancer. *J. Pharmacol. Exp. Ther.* **2015**, *353*, 392−404.
(94) Rello, S.; Stockert, J. C.; Moreno, V.; Gámez, A.; Pacheco, M.; Juarranz, A.; Cañete, M.; Villanueva, A. Morphological Criteria to Distinguish Cell Death Induced by Apoptotic and Necrotic Treatments. *Apoptosis* **2005**, *10*, 201−208.
(95) Bastian, A.; Matsuzaki, S.; Humphries, K. M.; Pharaoh, G. A.; Doshi, A.; Zaware, N.; Gangjee, A.; Ihnat, M. A. AG311, a Small Molecule Inhibitor of Complex I and Hypoxia-Induced HIF-1α Stabilization. *Cancer Lett.* **2017**, *388*, 149−157.
(96) Banerjee, S.; Pillai, M. R. A.; Ramamoorthy, N. Evolution of Tc-99m in Diagnostic Radiopharmaceuticals. *Semin. Nucl. Med.* **2001**, *31*, 260−277.
(97) Pashentsev, V. N. Current State and Prospects of Production of Radionuclide Generators for Medical Diagnosis. *Biomed. Eng.* **2016**, *49*, 340−343.
(98) Duatti, A.; Alberto, R.; Mindt, T. L.; Struthers, H.; Schibli, R.; Di Domenico, G.; Zavattini, G.; Pirmettis, I.; Pietzsch, H.-J.; Welling, M.; Ferro-Flores, G.; Wiebe, L. I.; Decristoforo, C.; Kuge, Y.; Akizama, H.; Uehara, T.; Arano, Y.; Ogawa, K.; Mallia, M. B.; Banerjee, S.; Venkatesh, M.; De Rosales, R. T. M.; Blower, P. *Technetium-99m Radiopharmaceuticals: Status and Trends,* 1st ed.; International Atomic Energy Agency: Vienna, Austria, 2009.
(99) Alberto, R.; Schibli, R.; Egli, A.; Schubiger, A. P.; et al. A Novel Organometallic Aqua Complex of Technetium for the Labeling of Biomolecules: Synthesis of $[^{99m}Tc(OH_2)_3(CO)_3]^+$ from $[^{99m}TcO_4]^-$ in Aqueous Solution and Its Reaction with a Bifunctional Ligand. *J. Am. Chem. Soc.* **1998**, *120*, 7987−7988.
(100) Yazdani, A.; Janzen, N.; Banevicius, L.; Czorny, S.; Valliant, J. F. Imidazole-Based [2 + 1] Re(I)/^{99m}Tc(I) Complexes as Isostructural Nuclear and Optical Probes. *Inorg. Chem.* **2015**, *54*, 1728−1736.
(101) Yazdani, A.; Janzen, N.; Czorny, S.; Valliant, J. F. Technetium-(I) Complexes of Bathophenanthrolinedisulfonic Acid. *Inorg. Chem.* **2017**, *56*, 2958−2965.
(102) Agilent Technologies UK Ltd. *CrysAlisPro;* Rigaku OD: The Woodlands, TX, 2015.
(103) Dolomanov, O. V.; Bourhis, L. J.; Gildea, R. J.; Howard, J. A. K.; Puschmann, H. *OLEX2*: A Complete Structure Solution, Refinement and Analysis Program. *J. Appl. Crystallogr.* **2009**, *42*, 339−341.
(104) Sheldrick, G. M. *SHELXT* − Integrated Space-Group and Crystal-Structure Determination. *Acta Crystallogr., Sect. A: Found. Adv.* **2015**, *A71*, 3−8.
(105) Sheldrick, G. M. A Short History of *SHELX*. *Acta Crystallogr., Sect. A: Found. Crystallogr.* **2008**, *A64*, 112−122.
(106) Müller, P. Practical Suggestions for Better Crystal Structures. *Crystallogr. Rev.* **2009**, *15*, 57−83.
(107) Thermo Scientific. *User Guide: Pierce BCA Protein Assay Kit;* Thermo Scientific: Rockford, IL, 2013.

DOI: 10.1021/acs.inorgchem.8b03552
Inorg. Chem. 2019, 58, 3895−3909